

CANDIDATE GRAVITATIONALLY LENSED DUSTY STAR-FORMING GALAXIES IN THE *HERSCHEL** WIDE AREA SURVEYS

H. NAYYER¹, M. KEELE¹, A. COORAY¹, D. A. RIECHERS², R. J. IVISON^{3,4}, A. I. HARRIS⁵, D. T. FRAYER⁶, A. J. BAKER⁷, S. C. CHAPMAN⁸, S. EALES⁹, D. FARRAH¹⁰, H. FU¹¹, L. MARCHETTI¹², R. MARQUES-CHAVES^{13,14}, P. I. MARTINEZ-NAVAJAS^{13,14}, S. J. OLIVER¹⁵, A. OMONT¹⁶, I. PEREZ-FOURNON^{13,14}, D. SCOTT¹⁷, M. VACCARI^{18,19}, J. VIEIRA²⁰, M. VIERO²¹, L. WANG²², J. WARDLOW^{23,24}

ABSTRACT

We present a list of candidate gravitationally lensed dusty star-forming galaxies (DSFGs) from the HerMES Large Mode Survey (HeLMS) and the *Herschel* Stripe 82 Survey (HerS). Together, these partially overlapping surveys cover 372 deg² on the sky. After removing local spiral galaxies and known radio-loud blazars, our candidate list of lensed DSFGs is composed of 77 sources with 500 μ m flux densities (S_{500}) greater than 100 mJy. Such sources are dusty starburst galaxies similar to the first bright Sub Millimeter Galaxies (SMGs) discovered with SCUBA. We expect a large fraction of this list to be strongly lensed, with a small fraction made up of bright SMG-SMG mergers that appear as Hyper-Luminous Infrared Galaxies (HyLIRGs; $L_{\text{IR}} > 10^{13} L_{\odot}$). Thirteen of the 77 candidates have spectroscopic redshifts from CO spectroscopy with ground-based interferometers, putting them at $z > 1$ and well above the redshift of the foreground lensing galaxies. The surface density of our sample is $0.21 \pm 0.03 \text{ deg}^{-2}$. We present follow-up imaging of a few of the candidates confirming their lensing nature. The sample presented here is an ideal tool for higher resolution imaging and spectroscopic observations to understand detailed properties of starburst phenomena in distant galaxies.

Subject headings: Gravitational lensing; strong – Submillimeter: galaxies

1. INTRODUCTION

Dusty Star-Forming Galaxies (DSFGs) are among the most intensely star forming systems in the Universe (see review by Casey et al. 2014). Optical studies of these galaxies are challenging, due to high dust obscuration that absorbs the rest-frame ultraviolet (UV) light emitted by young and hot stars. Instead these sources are bright at the longer wavelengths due to the emission from heated dust (Draine & Li 2001; Siebenmorgen et al. 2014). The far-infrared luminous DSFGs are bright in the sub-mm wavelengths and are similar to the first bright Sub Millimeter Galaxies (SMGs) discovered with SCUBA (Smail et al. 1997; Barger et al. 1998; Blain et al. 1999; Dunne et al. 2000; Chapman et al. 2005; Tacconi et al. 2006, 2008; Magnelli et al. 2012; Hayward et al. 2013; Swinbank et al. 2014; Wiklind et al. 2014; Ikarashi et al. 2015) with the brightest sources in the far-infrared bands (with infrared luminosities of $10^{12} L_{\odot} < L_{\text{IR}} < 10^{13} L_{\odot}$) classified as Ultra-Luminous Infrared Galaxies (ULIRGs; Sanders et al. 1988; Sanders & Mirabel 1996; Lutz et al. 1999; Alonso-Herrero et al. 2006; Clements et al. 2010; Kilerci Eser et al. 2014; Magdis et al. 2014). Resolved imaging of DSFGs at high redshifts is challenging, given the intrinsic faintness of such systems (with intrinsic flux densities of typically 10 mJy at 500 μ m, from models or direct observations

versity of Illinois, 1002 West Green St., Urbana, IL 61801

²¹ Department of Physics, Stanford University, Stanford, California 94305

²² SRON Netherlands Institute for Space Research, Landlevan 12, 9747 AD, Groningen, The Netherlands

²³ Dark Cosmology Centre, Niels Bohr Institute, University of Copenhagen, DK-2100 Copenhagen, Denmark

²⁴ Centre for Extragalactic Astronomy, Department of Physics, Durham University, South Road, Durham, DH1 3LE, UK

* *Herschel* is an ESA space observatory with science instruments provided by European-led Principal Investigator consortia and with important participation from NASA.

¹ Department of Physics & Astronomy, University of California, Irvine, CA 92697

² Department of Astronomy, Cornell University, Ithaca, NY, 14853

³ European Southern Observatory, Karl-Schwarzschild-Strasse 2, 85748 Garching, Germany

⁴ Institute for Astronomy, University of Edinburgh, Blackford Hill, Edinburgh EH9 3HJ, UK

⁵ Department of Astronomy University of Maryland College Park, MD 20742

⁶ National Radio Astronomy Observatory, Green Bank, WV, 24944

⁷ Department of Physics & Astronomy, Rutgers, the State University of New Jersey, 136 Frelinghuysen Road, Piscataway, NJ 08854-8019

⁸ Institute of Astronomy, University of Cambridge, Madingley Road, Cambridge, CB3 0HA, U.K.

⁹ School of Physics & Astronomy, Cardiff University, Cardiff, UK

¹⁰ Department of Physics, Virginia Polytechnic Institute and State University, Blacksburg, VA 24061

¹¹ Department of Physics & Astronomy, University of Iowa, Iowa City, Iowa 52242

¹² Department of Physical Sciences, The Open University, Milton Keynes, MK7 6AA, UK

¹³ Instituto de Astrofísica de Canarias, E-38205 La Laguna, Tenerife, Spain

¹⁴ Universidad de La Laguna, Dpto. Astrofísica, E-38206 La Laguna, Tenerife, Spain

¹⁵ Department of Physics & Astronomy, University of Sussex, Brighton BN1 9QH, UK

¹⁶ Institut d'Astrophysique de Paris, UMR 7095 CNRS, Université Pierre et Marie Curie, 75014, Paris, France

¹⁷ Department of Physics & Astronomy, University of British Columbia, 2329 West Mall, Vancouver, BC V6T 1Z4, Canada

¹⁸ Department of Physics and Astronomy, University of the Western Cape, Robert Sobukwe Road, 7535 Bellville, Cape Town, South Africa

¹⁹ INAF - Istituto di Radioastronomia, via Gobetti 101, 40129 Bologna, Italy

²⁰ Department of Astronomy and Department of Physics, Uni-

such as Ivison et al. 2010; Béthermin et al. 2012b,a or from lensing magnification corrected 500 μm studies such as Negrello et al. 2010; Wardlow et al. 2013) and/or large point spread functions of single dish diffraction-limited observations at sub-mm wavelengths. Although the latter is no longer a limitation, because of multi-dish observations such as with ALMA using long baselines (Karim et al. 2013; Wang et al. 2013; Riechers et al. 2014; Simpson et al. 2015b; ALMA Partnership et al. 2015a), the field of view remains limited to a few arcseconds (Karim et al. 2013). As a result, current studies of high-redshift DSFGs are generally limited to a small number of targets (Capak et al. 2008; Riechers et al. 2010, 2013; Fu et al. 2013; Riechers et al. 2014) and the most highly magnified star-forming systems (such as the Cosmic Eyelash; Swinbank et al. 2010b) or extreme starbursts (Coppin et al. 2009; Riechers et al. 2013; Gilli et al. 2014; De Breuck et al. 2014; Riechers et al. 2014).

Gravitational lensing provides a valuable tool to study galaxies that would otherwise be too distant or faint for current observational facilities (eg. Treu 2010; Treu & Ellis 2014). This is due to the fact that lensing enhances apparent angular size and magnifies source flux density (Richard et al. 2014; Atek et al. 2014), enabling studies of sources with intrinsic brightness below the nominal source detection limits of current facilities (Wardlow et al. 2013). By searching blank-field sub-millimeter surveys for bright sources, we can select galaxies that have a higher probability to be magnified by lensing (Swinbank et al. 2014; Simpson et al. 2015b,a). With the advent of large area far-infrared and sub-mm surveys it is now possible to search for bright sources as candidate gravitationally lensed systems with the selection based on the sub-mm flux density only (Negrello et al. 2007, 2010).

The *Herschel* Space Observatory (Pilbratt et al. 2010) provided us with a unique opportunity to study DSFGs at high redshift. This is possible through both large-area sky surveys, such as the *Herschel* Astrophysical Tera-hertz Large-Area Survey (H-ATLAS; Eales et al. 2010), and deeper observations but over smaller areas, such as those of the *Herschel* Multi-tiered Extragalactic Survey (HerMES; Oliver et al. 2012). The large area searches for gravitationally lensed systems has been very successful over the past few years at identifying high redshift DSFGs. In particular *Herschel* has been successful at identifying rare lensing systems, with some detailed studies already in the literature (Ivison et al. 2010; Cox et al. 2011; Fu et al. 2012; Messias et al. 2014). Follow-up observations of these candidates with ground-based facilities (such as ALMA; Messias et al. 2014; Schaerer et al. 2015) and the *Hubble* Space Telescope in the near-infrared has revealed the nature of the ISM in these systems with spatial resolutions at the level of 100 pc scales (Karim et al. 2013; Swinbank et al. 2014; Riechers et al. 2014; Swinbank et al. 2015). This allows us to study gas regulations and kinematics inside distant galaxies which sheds light on star formation mechanism and efficiency in the most gas-rich systems during the peak epoch of star formation in the Universe (Riechers et al. 2014). An interesting example is SDP.81, which was initially identified with *Herschel* during the Science Demonstration Phase (SDP; Negrello et al. 2010) as a lensed DSFG (Frayer et al. 2011; Hopwood et al. 2011; Negrello et al. 2014; Dye et al. 2014). SDP.81 was later used for Sci-

ence Verification observations of ALMA long baselines (ALMA Partnership et al. 2015b). Those data, collected for more than 30 hours, have now resulted in a robust lens model and have enabled ISM studies by revealing clumpy structures and giant molecular clouds within the lensed galaxy down to 80 pc scales (Dye et al. 2015; Wong et al. 2015; Swinbank et al. 2015; Rybak et al. 2015a,b; Hatsukade et al. 2015; Hezaveh et al. 2016).

The aim of this work is to expand the currently known samples of bright, lensed galaxies from *Herschel*. The first study of this kind used the Science Demonstration Phase map of H-ATLAS spanning 14 deg² in Negrello et al. (2010), identifying five candidate lenses that were confirmed to be lensed with follow-up data. The second systematic search for lensing systems in *Herschel* imaging data appeared in Wardlow et al. (2013), selecting 13 candidate lensed systems over 95 deg² of HerMES, composed of many smaller fields with individual sizes at the level of 2-10 deg². Among those 13, eleven are now confirmed as strong lens systems; the two remaining systems are luminous SMG-SMG mergers (Fu et al. 2013; Busmann et al. 2015).

Here we extend these two earlier studies with *Herschel*/SPIRE (Spectral and Photometric Imaging Receiver; Griffin et al. 2010) observations at 250, 350 and 500 μm to select potentially gravitationally lensed galaxies in the HerMES Large Mode Survey (HeLMS) and *Herschel* Stripe 82 Survey (HerS; Viero et al. 2014) fields. The *Herschel* HeLMS is a wide, SPIRE-only observations covering an area of 301 deg² in the SDSS Stripe 82 region with ancillary data from several facilities (Oliver et al. 2012, Clarke et al. 2016). The SPIRE observations reach a 5 σ limiting depth of 48 mJy in the 500 μm . The equatorial SDSS Stripe 82 HerS observations cover an area of 81 deg² with an average depth of 14.8 mJy beam⁻¹ (Viero et al. 2014, Clarke et al. 2016). This along with the ancillary data available in these equatorial fields, in particular deep SDSS observations from Stripe 82, enable us to identify and study these lensed galaxies.

The catalog presented here has *Herschel* photometry measured in the three SPIRE bands. Follow-up observations with the Keck/NIRC2 using Laser-guided adaptive optics (LGS-AO) and with the seeing-limited William Herschel Telescope (WHT) LIRIS near-IR imaging instrument reveal the lensing nature of several of these systems. We also present follow-up observations of some of these sources with mm-wave interferometric spectroscopy of CO emission lines to determine the redshift of background lensed galaxies. In particular, we present redshifts measured for targeted background lensed DSFGs with CO (1 \rightarrow 0) observations by the Green Bank Telescope (GBT)/Zpectrometer (Harris et al., in prep) and with multiple CO lines from Combined Array for Research in Millimeter-wave Astronomy (CARMA) and Plateau de Bure Interferometer (PdBI) (Riechers et al., in prep) showing that the confirmed lensed galaxies are at $z > 1$ with a target being at redshift as high as $z \sim 5$. The SDSS-detected foreground lensing galaxies have mean photometric redshifts peaking at $z \sim 0.4$ with spectroscopic observations for some of the targets confirming $z < 1$.

The paper is organized as follows. In Section 2, we discuss the lensed galaxy selection along with photometry

measurements. Section 3 describes some of the follow-up programs and existing results. We discuss our candidate lens sample, statistical properties and some example lensed sources in Section 4. We conclude with a summary in Section 5. Throughout this paper we assume a standard cosmology with $H_0 = 70 \text{ km s}^{-1} \text{ Mpc}^{-1}$, $\Omega_m = 0.3$ and $\Omega_\Lambda = 0.7$.

2. IDENTIFICATION OF CANDIDATE SOURCES

Our candidate lensed DSFGs are selected from HeLMS and HerS blank field data¹. HeLMS and HerS cover 301.3 and 80.5 deg^2 respectively, overlapping in a $\sim 10 \text{ deg}^2$ region. HeLMS is the widest area tier of HerMES (Oliver et al. 2012), the SPIRE Team’s Guaranteed Time Observations (GTO) with *Herschel* Space Observatory (Pilbratt et al. 2010). We use the maximum likelihood map-maker SANEPIC (Signal and Noise Estimation Procedure Including Correlations; Patanchon et al. 2008) to create our maps. We refer the reader to Asboth et al. (2016) and Clarke et al. (2016) for details related to HeLMS, data processing, and map making. Similar details related to HerS are available in Viero et al. (2014). The maps we produced are comparable in quality to publicly available maps from HerS, while for the HeLMS data we compare our maps to the results from the SMAP/SHIM iterative map maker (Levenson et al. 2010). The differences, if any, are at large angular scales related to the diffuse background. For point sources and point source flux estimation, the different maps showed a comparable performance within the uncertainties related to instrumental and confusion noise. The nominal pixel sizes at 250 , 350 and $500 \mu\text{m}$ are 6 , 8.3 and 12 arcseconds, respectively, matching one third of the full-width half-maximum (FWHM) of the beam in each band (18 , 25 , and 36 arcseconds respectively). We used and compared multiple catalogs as part of this study. The first set of catalogs make use of SUSSEXTRACTOR (Savage & Oliver 2007; Smith et al. 2012), available from the *Herschel* Interactive Processing Environment (HIPE; Ott 2010), based on sources detected at each of 250 , 350 and $500 \mu\text{m}$. The second set is discussed in Clarke et al. (2016) using STARFINDER and DESPHOT. The latter makes use of $250 \mu\text{m}$ detections to cross-identify and deblend at 350 and $500 \mu\text{m}$ flux densities, which reduces contamination from blended sources (XID catalogs).

Here we primarily focus on bright sources with flux densities above 100 mJy at $500 \mu\text{m}$. While our initial selection is with catalogs based on each of the wavelengths, using SUSSEXTRACTOR catalogs, the final selection involves removal of sources that are flagged as potentially blended systems using XID catalogs of Clarke et al. (2016). Unlike Clarke et al. (2016), which requires a $250 \mu\text{m}$ detection, we are able to search for and catalog lensed candidates that are also “red” with $S_{250} < S_{350} < S_{500}$ (Asboth et al. 2016). Bright $500 \mu\text{m}$ sources are dominated by gravitationally lensed galaxies, local spiral galaxies, and blazars (Negrello et al. 2010; Wardlow et al. 2013). Both local spirals and blazars can be excluded via cross-matching with shallow full sky surveys at optical and radio wavelengths, respectively. This method has been exploited recently in other *Herschel*

fields to select high-redshift gravitationally lensed galaxies (Negrello et al. 2010; Conley et al. 2011; González-Nuevo et al. 2012; Busmann et al. 2013; Wardlow et al. 2013; Negrello et al. 2014). After correction for contamination, this technique has been shown to be very successful at generating a robust catalog of gravitationally lensed high redshift galaxies (Negrello et al. 2010).

We remove local galaxies from our catalogs by searching the NASA/IPAC Extragalactic Database (NED) and the Sloan Digital Sky Survey III Data Release 12 at the $250 \mu\text{m}$ positions of our sources. Local galaxies are then recognized by visual inspection of the SDSS cutouts and identified by name in NED. There are 273 such sources in our fields, 231 from HeLMS and 44 from HerS (two lie in the overlapping region). These sources are all within 200 Mpc . As these local galaxies are rare (0.74 deg^{-2}) and occupy only a small portion of the fields, positional alignment between background dusty star-forming galaxies and these local galaxies should not be significant. Furthermore, the typical distance ratio between foreground and background population is such that, in the case of chance alignments, the foreground galaxy will not act as a strong gravitational lens. Hence we do not expect to lose bona fide strongly lensed galaxies by removing the local spirals. The relative colors of the local galaxies and lens candidates also typically occupy different regions of the color space. We also remove radio-loud blazars in a similar fashion, searching NED for all sources within 12 arcseconds of the position of the peak $500 \mu\text{m}$ flux. Sources identified as radio-loud quasars in previous surveys are then removed from our target list. We found nine blazars using this method. Note that our search was simply limited to known radio-loud blazars and we did not search for new blazar candidates. Given the existence of archival radio surveys down to sufficient depth we do not consider contamination from unknown blazars to be a significant issue with the candidate lensed sample.

After removal of the aforementioned contaminants, we examine our target lists from HeLMS and HerS for sources present in both catalogs from the 15 deg^2 region covered by both surveys. These duplicate sources are found by matching every source in the HeLMS catalog with the source with nearest position in HerS, as measured by peak S_{250} flux. The SPIRE observations at the $250 \mu\text{m}$ have better angular resolution ($\text{FWHM} = 18''$) compared to the redder bands which makes it more suitable for the cross-matching. Duplicate sources have a nominal separation that is small compared to the separation between sources that are merely nearby in a two-dimensional sky projection, between 1.3 and 7.2 arcseconds in all cases. In comparison, the closest two distinct sources in the combined catalog are separated by 45 arcseconds. The flux densities at 250 , 350 , and $500 \mu\text{m}$, and the colors of the sources, can also be compared to provide confirmation that sources from the two catalogs are indeed duplicates. Through this process, we found eight lens candidates that are present in both HeLMS and HerS, as well as the two local galaxies mentioned previously. In these cases, we remove the source from the HeLMS catalog and use the position and flux data from the deeper HerS data in all catalogs and analysis.

We next generate cut-outs at the positions of the peak S_{250} flux from the HeLMS and HerS maps at 250 , 350 ,

¹ <http://www.astro.caltech.edu/hers/Science.html>

and $500\ \mu\text{m}$ for all sources with $S_{500} > 100\ \text{mJy}$, which together define our primary lens candidate catalog. These cutouts are presented in the Appendix. From this list, we removed any remaining spatially extended sources and sources that are blended in S_{500} compared to the $250\ \mu\text{m}$ imaging. Extended sources that are bright at sub-millimeter wavelengths, but are not local galaxies, are primarily galactic cirrus clouds and are not of interest for this catalog (Low et al. 1984; Silva et al. 1998; Rowan-Robinson et al. 2014). We identify point sources that are separate by at least two beam sizes (separations $\sim 40''$) in the *Herschel*/SPIRE $250\ \mu\text{m}$ band. This should include any cluster lensed galaxies such as the HLSW-01 with a separation of $9''$, identified in the HerMES (Scott et al. 2011; Conley et al. 2011; Riechers et al. 2011; Gavazzi et al. 2011). We further cross matched our catalog of HeLMS/HerS sources with $S_{500} > 100\ \text{mJy}$ against the photometrically selected galaxy cluster catalog of Durret et al. (2015) in the Stripe 82. We found no cluster lensing systems within our $500\ \mu\text{m}$ bright sources.

As mentioned above one of the caveats of the SUSSEXTRACTOR catalogs is the difficulty in de-blending sources. In order to check the robustness of our bright $500\ \mu\text{m}$ lensed DSFG candidates we cross-checked our SUSSEXTRACTOR identified sources with the STARFINDER+ $250\ \mu\text{m}$ -detected XID catalog (Viero et al. 2014, Clarke et al. 2016), which used $250\ \mu\text{m}$ positions to de-blend $500\ \mu\text{m}$ flux densities. The only disadvantage of this catalog is that it relies on $250\ \mu\text{m}$ detections and thus does not contain $500\ \mu\text{m}$ peakers with faint $250\ \mu\text{m}$ emission. Using this combination of two catalogs we identified close to 30 sources that appear to be clear blends in $250\ \mu\text{m}$, but appear as a single source at $500\ \mu\text{m}$. Since they are likely multiple faint sources, rather than a single bright object, we do not consider such cases to be reliable candidates for gravitationally lensed sources. This approach, however, also results in a potential removal of rare lensed galaxies with image separations at the level of 30 arcseconds or more. Such lensing will involve most massive galaxy clusters in the foreground and are best searched for by combining SPIRE catalogs and known galaxy cluster positions. Given that our goal is to obtain a reliable list with high efficiency for lensing, and not necessarily a complete list of all lensed galaxies, we consider our approach to be adequate to increase the reliability that a higher fraction of the sources in our candidate list are gravitationally lensed DSFGs.

After removing blended sources, and sources that are extended - and thus likely to be contaminants from Galactic cirrus clumps (see Clarke et al. 2016) - we are left with a total of 77 lensed candidate galaxies with $S_{500} > 100\ \text{mJy}$ in our primary candidate list. The $S_{500} > 100\ \text{mJy}$ candidates have surface density $0.21 \pm 0.03\ \text{deg}^{-2}$ over the HeLMS and HerS fields. Using a sample of lensed DSFGs in the HerMES field Wardlow et al. (2013) measured a space density of $0.14\ \text{deg}^{-2}$ for systems with $S_{500} > 100\ \text{mJy}$ for a candidate lensed sample composed of 13 systems. Among the 13, two has since been identified to be SMG-SMG mergers, though in both cases, there is evidence for moderate lensing with magnification factors between 1.3 to 1.8 (Fu et al. 2013; Bussmann et al. 2015). With those two removed, the actual surface density of lensed galaxies with $S_{500} > 100\ \text{mJy}$ in HerMES

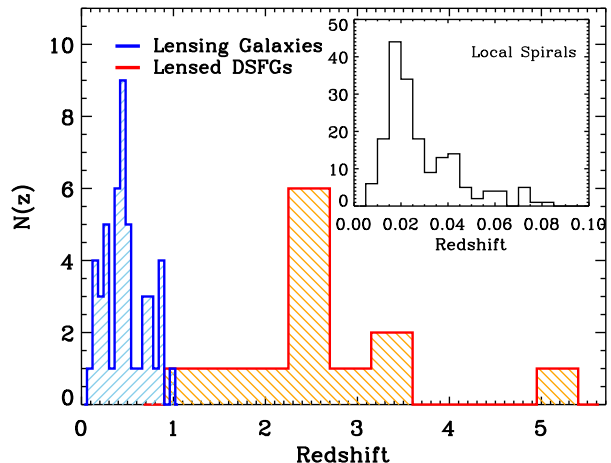


Figure 1. Redshift distribution of the thirteen HeLMS and HerS candidate lensed galaxies with spectroscopic redshifts from CO observations (Harris et al., in prep, Riechers et al., in prep). The DSFGs are at a median redshift of 2.51, while the foreground galaxies have median redshift of 0.44 putting the background lensed systems at much higher redshifts compared to the foreground lensing galaxies. The inset shows the redshift distribution of the local spiral galaxies that are bright in the $500\ \mu\text{m}$.

is around $0.11\ \text{deg}^{-2}$. This is substantially smaller than the surface density of our candidate list at $0.21\ \text{deg}^{-2}$. We expect that $\sim 15\%$ of our sample to be also composed of SMG-SMG mergers, similar to sources studied in Fu et al. (2013); Ivison et al. (2013). The real difference is likely due to cosmic variance. The study by Wardlow et al. (2013) involves multiple smaller legacy fields that were used in HerMES to form $95\ \text{deg}^2$. These extragalactic legacy fields, such as XMM-LSS or Boötes, are carefully selected to be devoid of known low- z ($z = 0.1 - 0.3$) massive galaxy clusters or galaxy over-densities that could potentially lens background DSFGs. Thus, these fields may, on average, provide a lower optical depth to lensing than a blank sky field. This is also visible in comparison to another result. The first lens selection with *Herschel*/SPIRE in H-ATLAS resulted in five confirmed lensed galaxies with a sky surface density of $0.35\ \text{deg}^{-2}$. While this area was $14\ \text{deg}^2$ it shows that large field-to-field variation in the number of lensed sources. This cosmic variance is a combination of spatial distribution of massive foreground galaxies or galaxy over-densities and the clustering of background DSFGs. With proper statistics on the lensed fraction from HeLMS and HerS, as well as the lensed sample over $650\ \text{deg}^2$ of H-ATLAS that is yet to fully appear in the literature, we expect it will be possible to observationally constrain the lensing optical depth variations of *Herschel*-selected DSFGs. A theoretical calculation of the expected cosmic variance will also be useful to address which parameters related to either the background DSFG population or foreground lenses can be constrained with such statistics.

Table 1 Cumulative number density of lensed sources.

Flux Limit $500\ \mu\text{m}$ (mJy)	Number Density (deg^{-2})	Low 68% [†] (deg^{-2})	High 68% [†] (deg^{-2})
100	0.207	0.186	0.233
110	0.153	0.136	0.176
120	0.102	0.088	0.121

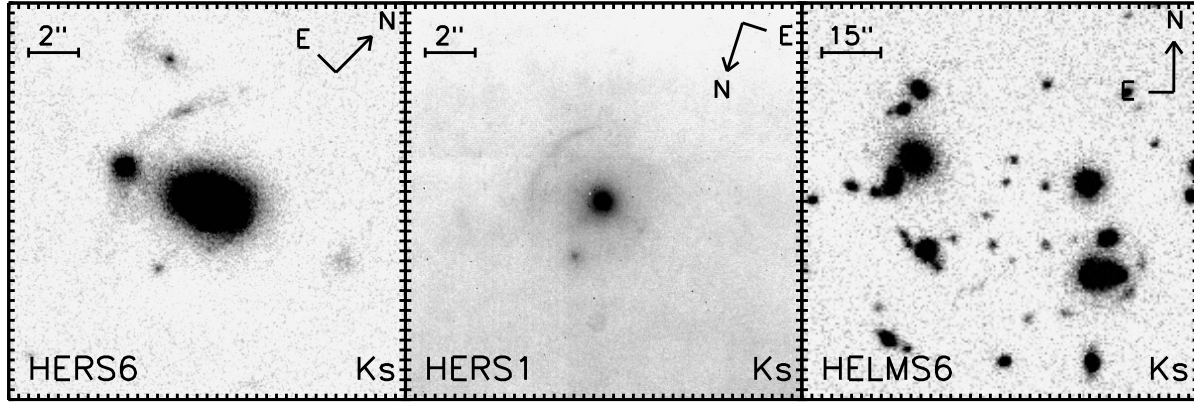


Figure 2. Keck/NIRC2 AO observations of two of our lensed DSFG candidates (HERS1 and HERS6) in the K_s band at $2.2\mu\text{m}$ along with William Herschel Telescope (WHT) LIRIS observations of HELMS6 in the K_s band. We clearly see lensing features in these three systems that were originally identified in the SPIRE $500\mu\text{m}$ band. HERS1 is the brightest source in our catalog at $500\mu\text{m}$ and it has been confirmed to be gravitationally lensed in a previous study by Geach et al. (2015) and recently with the Atacama Cosmology Telescope (Su et al. 2015).

130	0.073	0.061	0.089
140	0.056	0.047	0.072
150	0.043	0.035	0.057
160	0.035	0.028	0.047
170	0.030	0.023	0.041
180	0.027	0.021	0.038
200	0.019	0.014	0.029
250	0.011	0.008	0.019
260	0.008	0.006	0.016
270	0.005	0.004	0.012
710	0.0027	0.0019	0.0088

[†]: Confidence intervals are calculated following the prescription of Gehrels (1986).

3. FOLLOW-UP OBSERVATIONS

3.1. Redshifts

The redshifts of gas-rich DSFGs can be determined using CO rotational emission lines in radio observations. This method has been used extensively to measure the redshift of distant DSFGs (Greve et al. 2005; Swinbank et al. 2010a; Lupu et al. 2012; Harris et al. 2012; Weiß et al. 2013; George et al. 2013; Decarli et al. 2014; Canameras et al. 2015; Zavala et al. 2015). The CO molecular line observations are also used to study the physical properties of SMGs and DSFGs (Tacconi et al. 2006, 2008; Solomon & Vanden Bout 2005; Carilli & Walter 2013). In particular CO brightness and spatial distribution could be utilized to determine the total molecular gas content and extent, which is responsible for star formation, in these gas-rich systems (Narayanan et al. 2012; Fu et al. 2012, 2013). As part of existing programs to follow-up *Herschel*-selected bright lensed galaxies, we obtained radio/millimeter CO redshift measurements of 12 sources in our HeLMS+HerS sample with the Robert C. Byrd Green Bank Telescope (GBT; 7 sources; Harris et al., in prep.), the Combined Array for Research in Millimeter-wave Astronomy (CARMA; 12 sources; Riechers et al., in prep.), and the IRAM/Plateau de Bure Interferometer (PdBI; 11 sources; Riechers et al., in prep.), and one source (HELMS29) with spectro-

scopic observations from ALMA (Asboth et al. 2016). The 12 sources with redshifts reported here come from a large sample of lensed *Herschel* sources, involving all of the wide area *Herschel* fields. The CO sample follows no particular selection criterion apart from flexibility in scheduling with each of the facilities. The GBT observations target CO ($1 \rightarrow 0$) transition, however as discussed in Harris et al. (2012), it is also possible to have a GBT CO ($2 \rightarrow 1$) transition for systems at $5.1 < z < 8$ or a line from species other than the CO, however this would be unlikely given the photometric redshift distributions and the weak nature of the other line species (Harris et al. 2012). The lensed DSFG candidates with confirmed spectroscopic redshift from CO observations have $500\mu\text{m}$ fluxes exceeding 121 mJy with a median flux of 164 mJy in the $500\mu\text{m}$. The spectroscopic observations confirmed the brighter candidates in the far-infrared demonstrating increased chance of detection for brighter objects (Riechers et al., in prep, Harris et al., in prep).

Figure 1 shows the redshift distribution of the background DSFGs measured from CO. The measured redshifts of the background sources are at $z > 1$ and peak at $z \sim 2.5$. This result is consistent with other studies of SMG redshift distributions (Chapman et al. 2005; Harris et al. 2012; Bussmann et al. 2013, 2015). Figure 1 also shows the redshift distribution of the foreground lensing galaxies. This result is derived from public SDSS catalogs and is mostly for the brighter optical counterparts (due to limited spectroscopic depth). However our spectroscopic campaigns on the *Herschel* selected lensing systems have successfully measured the individual galaxy spectra using large ground-based observatories such as Keck (DEIMOS and LRIS) along with observations from Gemini, MMT and VLT (Bussmann et al. 2013). The redshift distribution of the foreground galaxies peaks at $z < 1$ and is consistent with the scenario that a background high redshift galaxy is being gravitationally lensed by a foreground system at much lower redshift.

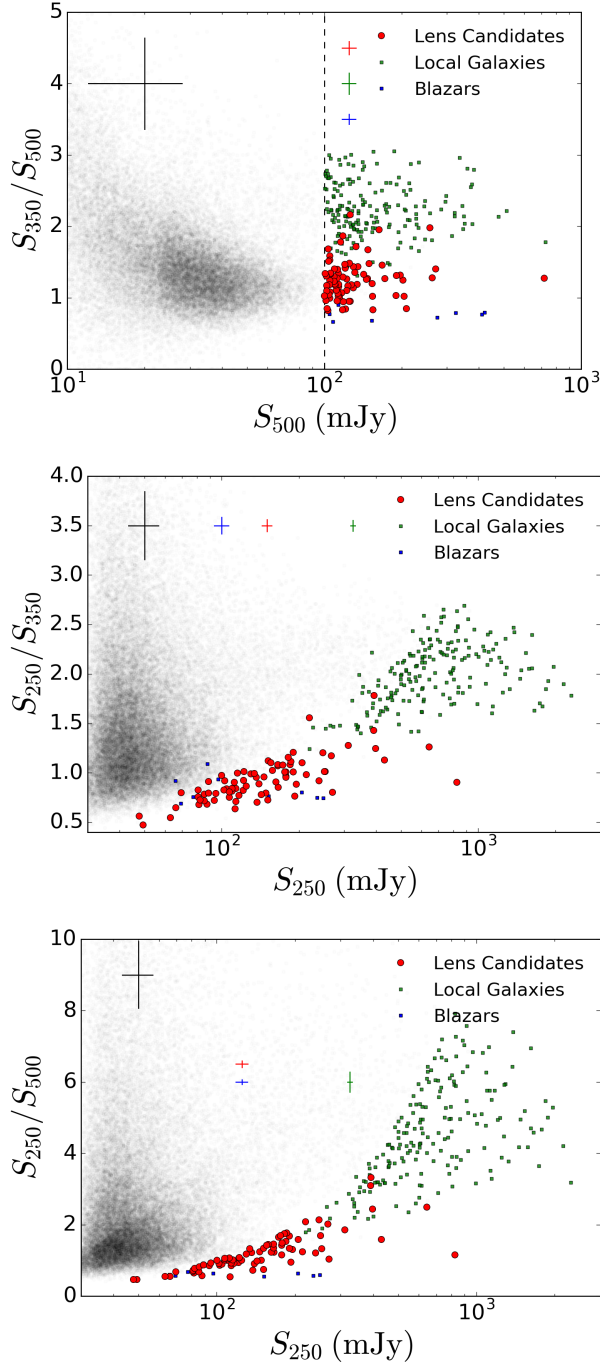


Figure 3. *Herschel*/SPIRE color vs. flux density plots for all sources in the HeLMS and HerS catalogs. Lens candidates, local galaxies, and blazars with $S_{500} > 100$ mJy are shown in color while all sources are shown in gray scale. Median error bars for all four populations are given at the top of the figures. The DSFGs in our gravitationally lensed candidate catalog are redder than the local galaxies, consistent with a greater redshift. The apparent offset of the lens candidates from the gray scale general population is due to our flux cut at $S_{500} = 100$ mJy and vanishes in the color-color plot (Figure 4).

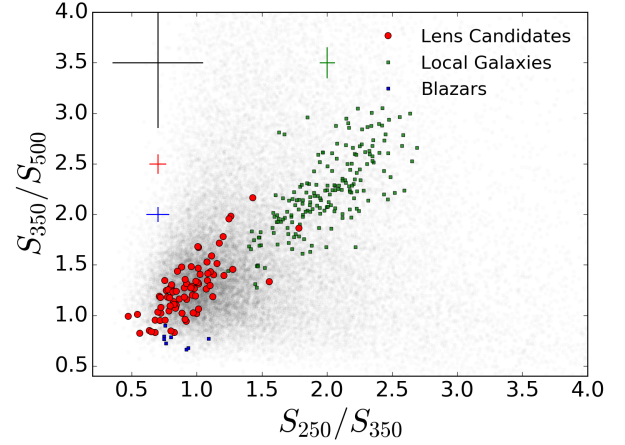


Figure 4. Color-color plot for all sources in the HeLMS and HerS catalogs. Sources with $S_{500} > 100$ mJy are highlighted when they belong to our lensing candidate, local galaxy, or blazar catalogs. The background gray scale shows the distribution of all sources in HeLMS and HerS. The colors of our candidate lensed DSFGs match those of the general HeLMS and HerS population. The error bars are standard deviations of the different populations.

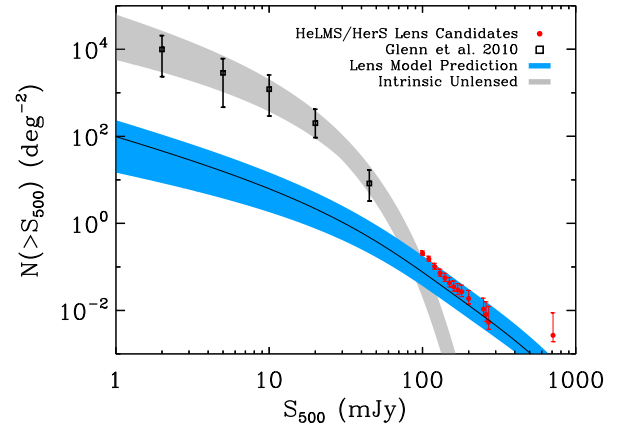


Figure 5. Cumulative 500 μ m number counts as a function of the *Herschel*/SPIRE 500 μ m flux. The lensed galaxy candidate counts from HerS and HeLMS are overlaid in red. These are consistent with counts of lensed sources as predicted from lensing statistics (Wardlow et al. 2013) shown with the black line with confidence interval in blue. For comparison we show the unlensed source counts from the HerMES blank-field catalogs (Oliver et al. 2012) and from P(D) analysis (Glenn et al. 2010) as grey shaded area and black squares respectively. The total counts of *Herschel* detected sources in these fields will be presented in future studies (Oliver et al., in prep, Clarke et al., in prep).

3.2. Imaging

As part of a “HELMS Deep” observing campaign, several of the lens candidates have been followed up with high resolution imaging with Keck/NIRC2 laser-guided adaptive optics (LGS AO) and with seeing limited imaging with the WHT LIRIS instrument in the near infrared. These observations were designed to study the rest-frame optical properties of these lensed systems in detail, as has been done over the past few years for other DSFGs at $z > 1$ (Fu et al. 2012, 2013; Calanog et al. 2014; Timmons et al. 2015). HELMS Deep observations of the lensed candidates were obtained with the Keck/NIRC2 AO sys-

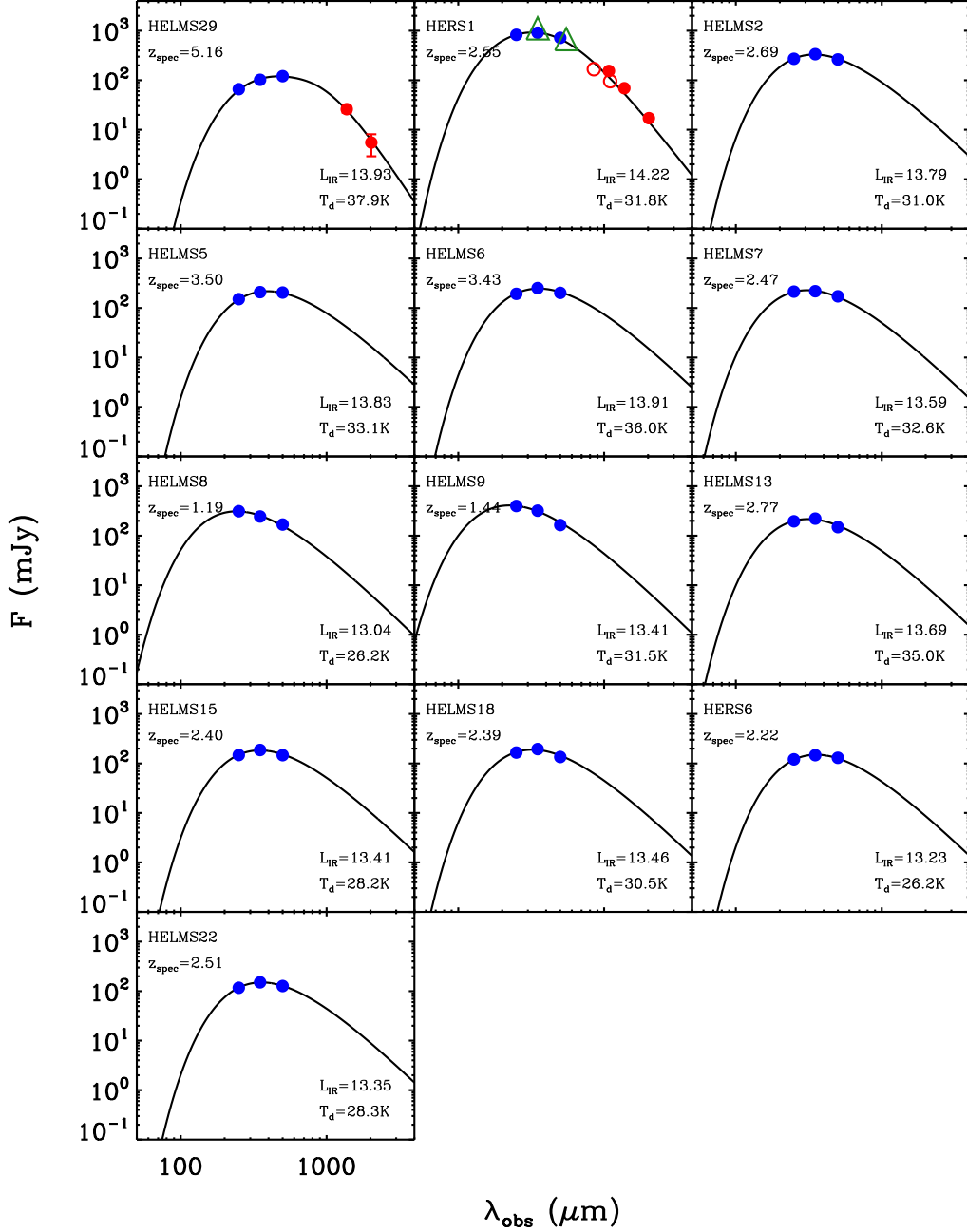


Figure 6. Far-infrared SED fits of the thirteen HerS and HeLMS lens candidates with CO spectroscopic redshifts using a modified black-body fit with $\beta = 1.5$ (Casey 2012). First two sources show mm-band observations from the Atacama Cosmology Telescope (Su et al. 2015) in filled red circles. HERS1 also has observations in mm-bands from Geach et al. (2015) (open circles) and also data from Planck point source catalog that is represented as open green triangles. The total infrared luminosity (integrated over 8-1000 μm in units of $\text{Log}(L_{\odot})$) and far infrared measured dust temperatures from the black-body fits (T_d) are also reported for each object.

tem in the K_s band at $2.2 \mu\text{m}$ in August and September of 2015 (PI: Cooray). The observations were done with an average exposure time of 3600 sec over two nights under cloudy conditions and poor AO correction. Figure 2 shows the KeckII/NIRC2-LGSAO K_s -band images of two of the lensed systems for which we obtained reliable data in these runs that are based on the new catalog presented here. The two galaxies (HERS1, discussed below and identified elsewhere as a lensing galaxy, and HERS6) both show clear lensing features in the near-infrared com-

posed of arcs and counter images. A detailed analysis of these imaging data, in combination with other multi-wavelength interferometric images, including those from an ALMA snapshot program (PI: Eales) will be presented in future papers. We highlight them here to motivate additional follow-up programs of the *Herschel* lens sample by the strong lensing community.

The WHT/LIRIS observations of HeLMS lens candidates are part of a Large Program on HerMES high-redshift galaxies (PI: Pérez-Fournon). The LIRIS ob-

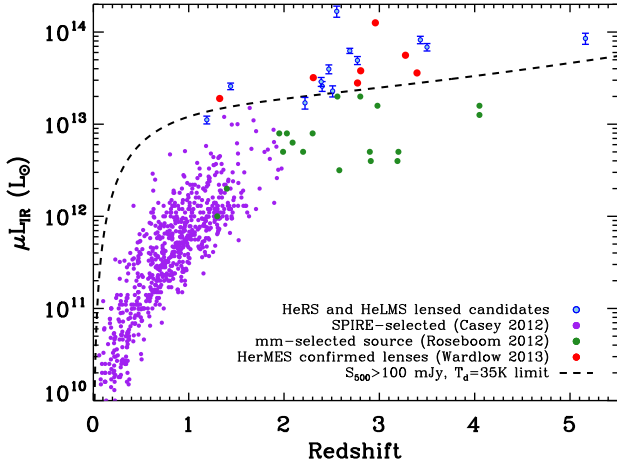


Figure 7. Total observed infrared luminosity (μ_{IR} ; rest-frame 8 – 1000 μm) measured from the *Herschel*/SPIRE data as a function of redshift. The DSFG redshifts are from spectroscopic CO observations by CARMA (Reichers et al., in prep) and the GBT (Harris et al., in prep). The curved dashed line shows the detection limit for our candidate lensed DSFGs from a modified blackbody model with $\beta = 1.5$, $T_d = 35$ K and 500 μm flux of 100 mJy similar to our selection flux cut (see Casey 2012). For comparison we are showing SPIRE-selected and mm-selected samples of star forming galaxies from Casey et al. (2012) and Roseboom et al. (2012) respectively. Candidate lensed DSFGs identified by Wardlow et al. (2013) are shown with filled red circles. At any given redshift, the lensed DSFGs would have a total infrared luminosity that exceeds those of red star forming galaxies because of the lensing magnification.

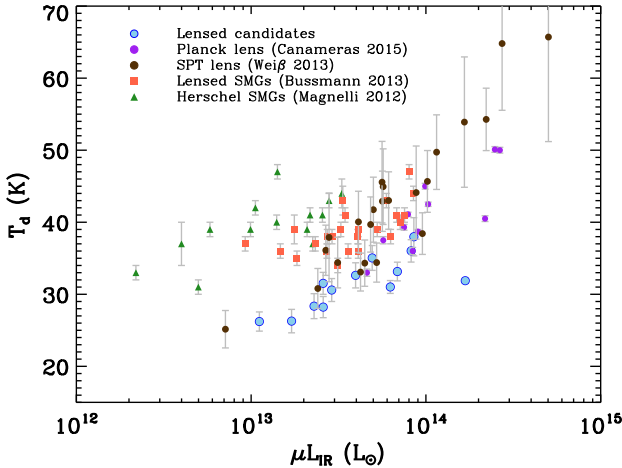


Figure 8. Dust temperature vs. total infrared luminosity for the candidate gravitationally lensed DSFGs in the HeLMS and HerS. The temperature and μ_{IR} (rest-frame 8 – 1000 μm) are plotted for a sub-sample of the lens candidates for which we have spectroscopic redshifts from CO observations by fitting a modified blackbody spectrum (see Casey 2012). The dust temperatures and infrared luminosities of several studies of lensed DSFGs and SMGs are shown for comparison (Magnelli et al. 2012; Bussmann et al. 2013; Weiß et al. 2013; Canameras et al. 2015). The smaller scatter in the derived dust temperatures is associated with the use of spectroscopic redshift information, from CO observations, in the SED fits. The lensed DSFGs have median dust temperatures of $T_d \sim 31$ K indicating a secular mode of star formation.

servations were done with a typical exposure time of 3600 sec in sub-arcsecond seeing conditions. Figure 2 also shows the WHT/LIRIS K_s imaging of HELMS6 observed on 26 October 2015, with seeing of 0.8". In this case, the main lensing galaxy is a member of a cluster of galaxies, with SDSS photometric redshift ~ 0.4 . Giant arcs are also present in this system. Optical long-slit spectroscopy of this field with the OSIRIS instrument of the Gran Telescopio Canarias (GTC) was obtained on 29 November 2015 in dark and clear conditions and seeing of 1.2 arcseconds. The exposure time was 3000 sec. We used the R1000B grism, with a spectral sampling of 2.12 \AA pixel $^{-1}$, and a slit width of 1.2 arcseconds. The slit included several of the galaxies in the cluster to the south of the main lensing galaxy. This position was chosen to include one of the lensed arc features. From these observations we could measure the spectroscopic redshifts of three galaxies in the cluster, of 0.3950, 0.3956, and 0.3968, close to the SDSS photometric redshift. More details and analysis will be presented in Marques-Chaves et al. (in prep).

4. DISCUSSION

4.1. Far-Infrared Colors

Figure 3 shows 250, 350, and 500 μm color-flux density plots for all sources detected in the HeLMS and HerS catalogs. Sources of interest, with $S_{500} > 100$ mJy, are highlighted in red, blue, and green, for our lens candidate galaxies, local galaxies, and blazars, respectively. As mentioned in Section 2, all flux measurements are taken from the HeLMS and HerS catalogs referenced above.

Our primary catalog of lensed DSFG candidate galaxies has median $S_{350}/S_{500} = 1.29 \pm 0.10$, $S_{250}/S_{350} = 0.90 \pm 0.06$, and $S_{250}/S_{500} = 1.16 \pm 0.09$ with errors being the standard deviation of the distribution. In comparison, the general population of all sources has median $S_{350}/S_{500} = 1.54 \pm 0.63$, $S_{250}/S_{350} = 1.34 \pm 0.33$, and $S_{250}/S_{500} = 2.06 \pm 0.80$. These have comparable colors, as expected, since the lensed candidates are drawn from the parent population of *Herschel* detected sources. The local galaxies have bluer colors than either the general population or our candidate lensed DSFGs, with median $S_{350}/S_{500} = 2.29 \pm 0.13$, $S_{250}/S_{350} = 2.07 \pm 0.08$, and $S_{250}/S_{500} = 4.74 \pm 0.27$. As this population is exclusively composed of galaxies at very low redshift, the relatively blue color is expected. The blazars have median $S_{350}/S_{500} = 0.68 \pm 0.08$, $S_{250}/S_{350} = 0.93 \pm 0.08$, and $S_{250}/S_{500} = 0.63 \pm 0.05$.

Our highlighted lens candidates, local galaxies, and blazars are offset from each other in the S_{250}/S_{350} vs S_{250} , S_{250}/S_{500} vs S_{250} , and S_{350}/S_{500} vs S_{500} color-flux space due to our selection criteria. Since we limited our search to sources bright in the S_{500} , which are correspondingly bright in the S_{250} , the highlighted sources all appear shifted to the right in Figure 3. As we see in Figure 4, this effect is not present in the color-color space where the distribution of candidate galaxies follows the general population.

4.2. Lensing Statistics

The statistics of lensing at sub-millimeter wavelengths has been discussed extensively in Perrotta et al. (2002); Negrello et al. (2007); Lima et al. (2010); Hezaveh &

Holder (2011); Wardlow et al. (2013), where similar techniques were used to identify lensed DSFGs in HerMES using *Herschel* 500 μm observations. The adopted model assumes a foreground mass profile and spatial distribution for the lensing galaxies, along with a redshift distribution of DSFGs with $S_{500} > 1 \text{ mJy}$, adopted from Béthermin et al. (2012a) for un-lensed DSFGs. The model ultimately makes predictions regarding the properties of lensed DSFGs (Wardlow et al. 2013). Figure 5 shows the cumulative 500 μm number counts of galaxies, considering the assumptions above. The cumulative number counts of lensed candidates are reported in Table 1. The confidence intervals in these measurements are calculated following the prescription of Gehrels (1986). We see a steep slope in the 500 μm number counts of un-lensed DSFGs, showing that the population of bright 500 μm sources should be dominated by gravitationally lensed objects along with bright local spirals in the 500 μm data (Wardlow et al. 2013).

According to the same lensing model, a 100 mJy flux cut produces a strong-lensing galaxy fraction of 32% – 74% (Wardlow et al. 2013) with an intrinsic flux density distribution that peaks at 5 mJy for the DSFGs. Given the HeLMS and HerS detection limits, many of these sources would be undetected without the magnification boost coming from lensing. Another prediction of this statistical model is that source blending does not significantly affect the lensed DSFG selection. This takes into account the blending of several intrinsically faint sources within the *Herschel* beam size that could produce a source with a combined flux above 100 mJy at 500 μm . Based on simulations, Wardlow et al. (2013) estimated that the blending of fainter galaxies has a probability of less than 5×10^{-5} to account for a source with flux density greater than 100 mJy. Within our sample of 77 lensed candidates, we do not expect a single source to result from the blending of two random fainter galaxies and still be identified as a single source. This is a result of the rarity of the bright DSFGs.

This estimate, however, ignores physical associations, rare instances of DSFG-DSFG mergers, or especially SMG-SMG mergers similar to the ones already uncovered with *Herschel* (eg. Fu et al. 2013; Ivison et al. 2013). Such sources are now believed to make up a considerable fraction of the $S_{500} > 100 \text{ mJy}$ population. Among the 13 lensed candidates in HerMES (Wardlow et al. 2013), one source was identified to be an SMG-SMG merger at $z = 2.3$ using the Sub-Millimeter Array (SMA) and other follow-up observations (HXMM01 of Fu et al. 2013). Using ALMA in Cycle 0 (see Bussmann et al. 2015) an additional source from the group of 13 was found to be a blend of at least three DSFGs that are weakly to moderately lensed (with $1 < \mu < 2$) by a low redshift galaxy that is 6 arcseconds away from the centroid of the three ALMA-detected sources. While we do not have precise predictions, we expect 10% – 15% of the sample to be SMG-SMG mergers. Detailed follow-up studies of the statistically significant sample presented here, involving a total of 77 lensed candidates, can be used to estimate the fraction more precisely. The exact fraction of SMG-SMG mergers, and their luminosity and mass distribution, is crucial for connecting such mergers with the formation history of the most massive and red galaxies at $z > 2$.

4.3. Luminosities and SEDs

For the subsample of lensed candidate DSFGs from HeLMS and HerS with CO-based redshifts, we deduce the observed total infrared luminosity (L_{IR} ; restframe 8-1000 μm) from the *Herschel*/SPIRE observations at 250, 350 and 500 μm using modified black-body fit to the data as explained in Casey (2012). The modified black-body takes into account variation in opacity and source emissivity. These fits are summarized in Figure 6. Two of the sources overlap with Su et al. (2015), as discussed below, and we include their flux densities. For one of the targets, HERS1, we also include Planck-detected flux densities.

Figure 7 shows μL_{IR} as a function of spectroscopic redshift measured from CO observations. The DSFGs have measured total infrared luminosities between $1.1 \times 10^{13} \mu^{-1} L_{\odot}$ and $1.6 \times 10^{14} \mu^{-1} L_{\odot}$ and a median of $4.9 \times 10^{13} \mu^{-1} L_{\odot}$. Using a Kennicutt (1998) relation for star formation ($\text{SFR}(M_{\odot} \text{yr}^{-1}) = 4.5 \times 10^{-44} L_{\text{IR}} (\text{ergs s}^{-1})$ with a Salpeter initial mass function; Salpeter 1955) we infer a median star formation rate of $\sim 8500 \mu^{-1} M_{\odot} \text{yr}^{-1}$. In the above μ is the gravitational lensing magnification for the *Herschel* selected lensed DSFGs. We can estimate the average maximum magnification as a function of the 500 μm flux from statistical gravitational lens modeling (Lapi et al. 2012; Wardlow et al. 2013) and direct observations of large SMA-detected samples of lensed DSFGs and SMGs (Bussmann et al. 2013). The measured infrared luminosities for these targets far exceed those of normal star-forming and IR luminous systems, providing further evidence of gravitational lensing, which is consistent with previous studies of lensed DSFGs (Wardlow et al. 2013). In fact, given the average magnification for bright gravitationally lensed sources (Wardlow et al. 2013; Bussmann et al. 2013) we infer a total infrared luminosity of lensed DSFGs consistent with that of normal IR-bright galaxies at similar redshifts.

Figure 8 shows the dust temperature, derived from SED fits described above, as a function of the total infrared luminosity for our lensed DSFG candidates with spectroscopic redshifts in the HeLMS and HerS fields. The candidate lensed systems have observed dust temperatures $\sim 25 - 40 \text{ K}$ and total observed luminosities (μL_{IR}) as reported above. Figure 8 also shows the dust temperature and infrared luminosities of other samples of lensed DSFGs and SMGs from the literature (Magnelli et al. 2012; Weiß et al. 2013; Bussmann et al. 2013; Canameras et al. 2015) where we have converted the intrinsic values to observed properties given the derived magnifications in those studies. The spread in the distribution of these sources on the T_d vs μL_{IR} plane is mostly associated with the different selection functions and also intrinsic properties of each population. Our candidate DSFGs show a smaller scatter in the measured properties which is mainly associated with the use of the redshift information (from the CO observations) for these systems in our SED fits (Magnelli et al. 2012). Our DSFG candidates have median SED measured dust temperatures of $T_d \sim 31 \text{ K}$. This indicates that our candidate DSFGs are more dominated by systems with cooler dust temperatures which is more consistent with secular modes of

star formation rather than merger driven star formation activity (Magnelli et al. 2012), also evident from our high resolution follow-up observations.

4.4. Example Lensed Sources

HERS1, shown in Figure 2, had been already identified as a lensed galaxy by a citizen science group SPACEWARPS making use of VISTA-CFHT optical imaging data in SDSS Stripe 82 (Geach et al. 2015). It is the brightest target in our list of 77 with a $500\ \mu\text{m}$ flux density of 717 mJy. It is a unique source in that it stands out at the bright-end separately on its own while the next set of lensed candidate sources have flux densities well below 300 mJy. The Keck/NIRC2 LGS-AO HELMS Deep K_s -band we present in Figure 2, obtained prior to us knowing about the SPACEWARPS project and the Geach et al. (2015) publication, has substantially better resolution than VISTA-CFHT K_s -band image in Geach et al. (2015). Unlike our previous lens follow-up programs in the K -band that resulted in the need for deep integrations due to faintness of the lensed source, HERS1 is bright enough in the K -band that the lensing galaxy is easily visible in a single NIRC2 frame of 60 seconds.

Additional multi-wavelength observations of this target, including CO spectroscopy, is reported in Geach et al. (2015). HERS1 is also detected in Planck all-sky point source catalog and is identified as PCCS2 857 G160.58-56.76 in the Planck 857 GHz point source catalog with a separation of less than 1 arcminute from the *Herschel*/SPIRE $250\ \mu\text{m}$ position, which is smaller than full-width-half-maximum (FWHM) resolution of the Planck ($\sim 4'$) at 857 GHz. The Planck has a 857 GHz flux of 1118 ± 408 mJy and a 545 GHz flux of 676 ± 197 mJy. These flux densities are consistent with the SPIRE $350\ \mu\text{m}$ and $500\ \mu\text{m}$ flux of 912 ± 7 mJy and 718 ± 8 mJy, respectively. The SED is shown in Figure 6. Fixing $\beta = 1.5$ does not provide a good fit for HERS1 given the additional data that we have, in particular at longer wavelengths. We kept β as a free parameter (Casey 2012) while fitting the full SED of HERS1 with *Herschel*/SPIRE, Planck and ACT data, giving a $\beta = 1.9$ and providing a better fit.

In a recent study Su et al. (2015) identified a sample of nine gravitationally lensed DSFGs using the Atacama Cosmology Telescope (ACT) in Stripe 82. Six of the nine lensing galaxies have $S_{500} > 100$ mJy. We had independently selected these six candidates in our sample, prior to our knowledge of the Su et al. (2015) study or preprint, in the current sample of HerS/HeLMS candidate gravitationally lensed galaxies. The three targets not selected in our study have $S_{500} < 100$ mJy and fall outside our lensed DSFG candidate selection. The far-infrared fluxes of all the 12 ACT candidates are consistent with the *Herschel*/SPIRE fluxes of the corresponding sources in our catalog, given the errors and the leeway in the SED fits. Two of the ACT detected lensed galaxies in our catalog (HERS1 and HELMS29) have spectroscopic redshift from CO observations (Harris et al in prep, Riechers et al in prep). HELMS29 at $z = 5.162$ (see below) is the highest redshift lensing galaxy in our sample. We use this redshift along with the *Herschel* far-infrared and ACT mm data to construct the SED (Figure 6). Similar to HERS1, discussed above, we treated β as a free parameter in the SED fit of HELMS29. The addition of ACT

data provided a better fit to the flux densities at longer wavelengths with a $\beta = 2.6$ (for more details on the fitting procedure see: Casey 2012). Su et al. (2015) also presents deep follow-up observations of their lensing sample, including CO redshift of one additional source (their other redshift is for HERS1). Unfortunately that source does not fall within the $S_{500} > 100$ mJy limit we have used in the present catalog. These independent follow-up campaigns by different groups (which we label as “battle of HELMS deep”) will likely result in additional redshifts for the lens galaxy sample we have presented here.

Asboth et al. (2016) discuss the “red” galaxies in HeLMS with $S_{500} > S_{350} > S_{250}$. Such a selection identifies candidate SMGs with $z > 4$, similar to the selection that led to HFLS3 (Riechers et al. 2013; Cooray et al. 2014), as discussed in Dowell et al. (2014). Six targets overlap between the two samples and are identified here in Table 2. These sources are likely to be lensed galaxies with $z > 4$. One such candidate, HELMS29, has a CO-based redshift of 5.162 and is discussed in detail in Asboth et al. (2016). The redshift is also confirmed by an ALMA Cycle 1 observation (PI: Conley), as discussed in Asboth et al. (2016). The HeLMS and HerS candidate list presented here is also part of a ALMA Cycle 2 snapshot program (PI: Eales). Ten of the targets from the HeLMS list have secured observations at 350 GHz and those targets are identified in Table 2. The ALMA data, lensing models, and multi-wavelength analysis will be presented in future papers.

5. SUMMARY AND CONCLUSIONS

We used *Herschel*/SPIRE maps of HeLMS and HerS surveys to produce a list of candidate gravitationally lensed DSFGs. Our main findings are:

- We identified 77 candidate lensed dusty star forming galaxies in the combined $372\ \text{deg}^2$ region covered by the *Herschel* HeLMS and HerS fields ($0.21 \pm 0.03\ \text{deg}^{-2}$).
- Candidate DSFGs are bright in the SPIRE $500\ \mu\text{m}$ observations ($S_{500} > 100$ mJy by selection). We further show that the colors of our candidate DSFGs are redder than the local spiral galaxies, indicative of a separate population at high redshift.
- Few of our brighter lensed DSFGs with red SEDs in the HeLMS field have been recently discovered in a parallel study (Asboth et al. 2016). The Atacama Cosmology Telescope (ACT) also confirmed the existence of a small sub-sample of our lensed DSFG candidates (Su et al. 2015). This further demonstrates the robustness of our selection of high redshift lensed galaxies.
- High resolution near-infrared follow-up observations of a few of the candidates with Keck/NIRC2 AO and William Herschel Telescope (WHT) reveal arcs and distorted images associated with gravitational lensing.
- Spectroscopic redshifts measured from CO molecular line observations (Harris et al., in prep; Riechers et al., in prep) for thirteen of the candidates put the population of lensed DSFGs at $z > 1$ whereas

the foreground lensing galaxies have redshift distribution that peaks at $z < 1$. This further supports the scenario of a population of distant objects being gravitationally lensed by nearby foreground galaxies.

- We fit the far-infrared SED of the candidate lensed DSFGs with modified black-body which gives us the best-fit total infrared luminosity (L_{IR} ; rest-frame 8–1000 μm) and dust temperature (T_{d}). For the SED fittings we fix the redshift of the galaxy to spectroscopic redshifts from CO observations. Two of the candidate DSFGs (HERS1 and HELMS29) also have longer wavelength data from ACT observations with HERS1 being also detected in the Planck point source catalog. We use these additional data in our SED analysis.
- The lensed DSFGs have median total infrared luminosities of $4.9 \times 10^{13} \mu^{-1} L_{\odot}$ where μ is the gravitational lensing magnification factor. The observed infrared luminosity for lensed DSFGs far exceeds that of normal star forming galaxies at similar redshifts. In fact given the average magnification for bright gravitationally lensed sources (Bussmann et al. 2013) we infer a total infrared luminosity of lensed DSFGs consistent with that of normal IR-bright galaxies at similar redshifts.
- The candidate lensed galaxies have SED measured dust temperatures in the range of $25 \text{ K} < T_{\text{d}} < 38 \text{ K}$ with a median of $T_{\text{d}} \sim 31 \text{ K}$ and a small scatter given the spectroscopic CO information. The relatively low dust temperature compared to the merger-driven dust temperatures in the IR luminous galaxies at similar redshifts supports the secular star formation evolution within these systems.

Given the high success rate of high redshift DSFG observations selected similarly from other studies Negrello et al. (2010); Wardlow et al. (2013) and from our own follow-up high resolution observations, we can conclude that the present catalog is a robust list of bona-fide gravitationally lensed galaxies at $z > 1$. About 10% to 15% of the sample is likely luminous SMG-SMG mergers that are of interest for understanding the formation paths of massive galaxies at $z > 2$. The lensing nature, properties of the lensed galaxies, and identification of SMG-SMG mergers for further studies will require carefully planned follow-up campaigns with a variety of facilities in the future.

ACKNOWLEDGEMENT

We wish to thank the anonymous referee for thoroughly reading the manuscript and providing very useful suggestions. Financial support for this work was provided by NSF through AST-1313319 for HN and AC and NSF REU support in AST-1313319 for MK. UCI group also acknowledges NASA support for *Herschel*/SPIRE GTO and Open-Time Programs. RJI acknowledges support from the European Research Council in the form of the Advanced Investigator Programme, 321302, COSMICISM. JLW is supported by a European Union COFUND/Durham Junior Research Fellowship

under EU grant agreement number 267209, and acknowledges additional support from STFC (ST/L00075X/1). Support for IPF, PIMN and RMS was from the Spanish MINECO grants AYA2010-21697-C05-4, FIS2012-39162-C06-02, and ESP2013-47809-C3-3-R. SO acknowledges support from the Science and Technology Facilities Council (grant number ST/L000652/1). The research leading to these results has received funding from the European Union Seventh Framework Programme FP7/2007-2013/ under grant agreement n° 607254. Disclaimer: “This publication reflects only the author’s view and the European Union is not responsible for any use that may be made of the information contained therein.” Some of the data presented herein were obtained at the W.M. Keck Observatory, which is operated as a scientific partnership among the California Institute of Technology, the University of California and the National Aeronautics and Space Administration. The Observatory was made possible by the generous financial support of the W.M. Keck Foundation. The authors wish to recognize and acknowledge the very significant cultural role and reverence that the summit of Mauna Kea has always had within the indigenous Hawaiian community. We are most fortunate to have the opportunity to conduct observations from this mountain. Data presented herein were obtained using the UCI Remote Observing Facility, made possible by a generous gift from John and Ruth Ann Evans. The *Herschel* spacecraft was designed, built, tested, and launched under a contract to ESA managed by the *Herschel*/Planck Project team by an industrial consortium under the overall responsibility of the prime contractor Thales Alenia Space (Cannes), and including Astrium (Friedrichshafen) responsible for the payload module and for system testing at spacecraft level, Thales Alenia Space (Turin) responsible for the service module, and Astrium (Toulouse) responsible for the telescope, with in excess of a hundred subcontractors. HCSS / HSpot / HIPE is a joint development (are joint developments) by the *Herschel* Science Ground Segment Consortium, consisting of ESA, the NASA *Herschel* Science Center, and the HIFI, PACS and SPIRE consortia. The IRAM Plateau de Bure Interferometer is supported by INSU/CNRS (France), MPG (Germany), and IGN (Spain). The National Radio Astronomy Observatory is a facility of the National Science Foundation operated by Associated Universities, Inc. Support for CARMA construction was derived from the Gordon and Betty Moore Foundation, the Kenneth T. and Eileen L. Norris Foundation, the James S. McDonnell Foundation, the Associates of the California Institute of Technology, the University of Chicago, the states of California, Illinois, and Maryland, and the National Science Foundation. Ongoing CARMA development and operations are supported by NSF grant ATI-0838178 to CARMA, and by the CARMA partner universities. The William Herschel telescope is operated on the island of La Palma by the Isaac Newton Group in the Spanish Observatorio del Roque de los Muchachos of the Instituto de Astrofísica de Canarias. Based in part on observations made with the Gran Telescopio Canarias (GTC), installed at the Spanish Observatorio del Roque de los Muchachos of the Instituto de Astrofísica de Canarias, in the island of La Palma.

REFERENCES

- ALMA Partnership et al. 2015a, *ApJ*, 808, L1
— 2015b, *ApJ*, 808, L4
Alonso-Herrero, A., et al. 2006, *ApJ*, 640, 167
Asboth, V., et al. 2016, *ArXiv e-prints*
Atek, H., et al. 2014, *ApJ*, 786, 60
Barger, A. J., Cowie, L. L., Sanders, D. B., Fulton, E., Taniguchi, Y., Sato, Y., Kawara, K., & Okuda, H. 1998, *Nature*, 394, 248
B  thermin, M., et al. 2012a, *ApJ*, 757, L23
— 2012b, *A&A*, 542, A58
Blain, A. W., Smail, I., Ivison, R. J., & Kneib, J.-P. 1999, *MNRAS*, 302, 632
Bussmann, R. S., et al. 2013, *ApJ*, 779, 25
— 2015, *ApJ*, 812, 43
Calanog, J. A., et al. 2014, *ApJ*, 797, 138
Canameras, R., et al. 2015, *ArXiv e-prints*
Capak, P., et al. 2008, *ApJ*, 681, L53
Carilli, C. L., & Walter, F. 2013, *ARA&A*, 51, 105
Casey, C. M. 2012, *MNRAS*, 425, 3094
Casey, C. M., Narayanan, D., & Cooray, A. 2014, *Phys. Rep.*, 541, 45
Casey, C. M., et al. 2012, *ApJ*, 761, 140
Chapman, S. C., Blain, A. W., Smail, I., & Ivison, R. J. 2005, *ApJ*, 622, 772
Clements, D. L., Dunne, L., & Eales, S. 2010, *MNRAS*, 403, 274
Conley, A., et al. 2011, *ApJ*, 732, L35
Cooray, A., et al. 2014, *ApJ*, 790, 40
Coppin, K. E. K., et al. 2009, *MNRAS*, 395, 1905
Cox, P., et al. 2011, *ApJ*, 740, 63
De Breuck, C., et al. 2014, *A&A*, 565, A59
Decarli, R., et al. 2014, *ApJ*, 782, 78
Dowell, C. D., et al. 2014, *ApJ*, 780, 75
Draine, B. T., & Li, A. 2001, *ApJ*, 551, 807
Dunne, L., Eales, S., Edmunds, M., Ivison, R., Alexander, P., & Clements, D. L. 2000, *MNRAS*, 315, 115
Durret, F., et al. 2015, *A&A*, 578, A79
Dye, S., et al. 2014, *MNRAS*, 440, 2013
— 2015, *MNRAS*, 452, 2258
Eales, S., et al. 2010, *PASP*, 122, 499
Frayser, D. T., et al. 2011, *ApJ*, 726, L22
Fu, H., et al. 2012, *ApJ*, 753, 134
— 2013, *Nature*, 498, 338
Gavazzi, R., et al. 2011, *ApJ*, 738, 125
Geach, J. E., et al. 2015, *MNRAS*, 452, 502
Gehrels, N. 1986, *ApJ*, 303, 336
George, R. D., et al. 2013, *MNRAS*, 436, L99
Gilli, R., et al. 2014, *A&A*, 562, A67
Glenn, J., et al. 2010, *MNRAS*, 409, 109
Gonz  lez-Nuevo, J., et al. 2012, *ApJ*, 749, 65
Greve, T. R., et al. 2005, *MNRAS*, 359, 1165
Griffin, M. J., et al. 2010, *A&A*, 518, L3
Harris, A. I., et al. 2012, *ApJ*, 752, 152
Hatsukade, B., Tamura, Y., Iono, D., Matsuda, Y., Hayashi, M., & Oguri, M. 2015, *PASJ*, 67, 93
Hayward, C. C., Narayanan, D., Kere  , D., Jonsson, P., Hopkins, P. F., Cox, T. J., & Hernquist, L. 2013, *MNRAS*, 428, 2529
Hezaveh, Y. D., & Holder, G. P. 2011, *ApJ*, 734, 52
Hezaveh, Y. D., et al. 2016, *ArXiv e-prints*
Hopwood, R., et al. 2011, *ApJ*, 728, L4
Ikarashi, S., et al. 2015, *ApJ*, 810, 133
Ivison, R. J., et al. 2010, *A&A*, 518, L35
— 2013, *ApJ*, 772, 137
Jiang, L., et al. 2014, *ApJS*, 213, 12
Karim, A., et al. 2013, *MNRAS*, 432, 2
Kennicutt, Jr., R. C. 1998, *ARA&A*, 36, 189
Kilerci Eser, E., Goto, T., & Doi, Y. 2014, *ApJ*, 797, 54
Lang, D. 2014, *AJ*, 147, 108
Lapi, A., Negrello, M., Gonz  lez-Nuevo, J., Cai, Z.-Y., De Zotti, G., & Danese, L. 2012, *ApJ*, 755, 46
Levenson, L., et al. 2010, *MNRAS*, 409, 83
Lima, M., Jain, B., & Devlin, M. 2010, *MNRAS*, 406, 2352
Low, F. J., et al. 1984, *ApJ*, 278, L19
Lupu, R. E., et al. 2012, *ApJ*, 757, 135
Lutz, D., Veilleux, S., & Genzel, R. 1999, *ApJ*, 517, L13
Magdis, G. E., et al. 2014, *ApJ*, 796, 63
Magnelli, B., et al. 2012, *A&A*, 539, A155
Messias, H., et al. 2014, *A&A*, 568, A92
Narayanan, D., Krumholz, M. R., Ostriker, E. C., & Hernquist, L. 2012, *MNRAS*, 421, 3127
Negrello, M., Perrotta, F., Gonz  lez-Nuevo, J., Silva, L., de Zotti, G., Granato, G. L., Baccigalupi, C., & Danese, L. 2007, *MNRAS*, 377, 1557
Negrello, M., et al. 2010, *Science*, 330, 800
— 2014, *MNRAS*, 440, 1999
Oliver, S. J., et al. 2012, *MNRAS*, 424, 1614
Ott, S. 2010, in *Astronomical Society of the Pacific Conference Series*, Vol. 434, *Astronomical Data Analysis Software and Systems XIX*, ed. Y. Mizumoto, K.-I. Morita, & M. Ohishi, 139
Patanchon, G., et al. 2008, *ApJ*, 681, 708
Perrotta, F., Baccigalupi, C., Bartelmann, M., De Zotti, G., & Granato, G. L. 2002, *MNRAS*, 329, 445
Pilbratt, G. L., et al. 2010, *A&A*, 518, L1
Richard, J., et al. 2014, *MNRAS*, 444, 268
Riechers, D. A., Hodge, J., Walter, F., Carilli, C. L., & Bertoldi, F. 2011, *ApJ*, 739, L31
Riechers, D. A., et al. 2010, *ApJ*, 720, L131
— 2013, *Nature*, 496, 329
— 2014, *ApJ*, 796, 84
Roseboom, I. G., et al. 2012, *MNRAS*, 419, 2758
Rowan-Robinson, M., et al. 2014, *MNRAS*, 445, 3848
Rybak, M., McKean, J. P., Vegetti, S., Andreani, P., & White, S. D. M. 2015a, *MNRAS*, 451, L40
Rybak, M., Vegetti, S., McKean, J. P., Andreani, P., & White, S. D. M. 2015b, *MNRAS*, 453, L26
Salpeter, E. E. 1955, *ApJ*, 121, 161
Sanders, D. B., & Mirabel, I. F. 1996, *ARA&A*, 34, 749
Sanders, D. B., Soifer, B. T., Elias, J. H., Madore, B. F., Matthews, K., Neugebauer, G., & Scoville, N. Z. 1988, *ApJ*, 325, 74
Savage, R. S., & Oliver, S. 2007, *ApJ*, 661, 1339
Schaerer, D., et al. 2015, *A&A*, 576, L2
Scott, K. S., et al. 2011, *ApJ*, 733, 29
Siebenmorgen, R., Voshchinnikov, N. V., & Bagnulo, S. 2014, *A&A*, 561, A82
Silva, L., Granato, G. L., Bressan, A., & Danese, L. 1998, *ApJ*, 509, 103
Simpson, J. M., et al. 2015a, *ApJ*, 807, 128
— 2015b, *ApJ*, 799, 81
Smail, I., Ivison, R. J., & Blain, A. W. 1997, *ApJ*, 490, L5
Smith, A. J., et al. 2012, *MNRAS*, 419, 377
Solomon, P. M., & Vanden Bout, P. A. 2005, *ARA&A*, 43, 677
Su, T., et al. 2015, *ArXiv e-prints*
Swinbank, A. M., et al. 2010a, *MNRAS*, 405, 234
— 2010b, *Nature*, 464, 733
— 2014, *MNRAS*, 438, 1267
— 2015, *ApJ*, 806, L17
Tacconi, L. J., et al. 2006, *ApJ*, 640, 228
— 2008, *ApJ*, 680, 246
Timmons, N., et al. 2015, *ApJ*, 805, 140
Treu, T. 2010, *ARA&A*, 48, 87
Treu, T., & Ellis, R. S. 2014, *ArXiv e-prints*
Viero, M. P., et al. 2014, *ApJS*, 210, 22
Wang, R., et al. 2013, *ApJ*, 773, 44
Wardlow, J. L., et al. 2013, *ApJ*, 762, 59
Wei  , A., et al. 2013, *ApJ*, 767, 88
Wiklind, T., et al. 2014, *ApJ*, 785, 111
Wong, K. C., Suyu, S. H., & Matsushita, S. 2015, *ApJ*, 811, 115
Wright, E. L., et al. 2010, *AJ*, 140, 1868
Zavala, J. A., et al. 2015, *MNRAS*, 452, 1140

APPENDIX

Table 2 HeLMS lens candidates ($S_{500} > 100$ mJy)

Object ID	RA	Dec	S_{250} (mJy)	S_{350} (mJy)	S_{500} (mJy)
HELMS1	23 ^h 34 ^m 41 ^s .0	−06°52′20″	431 ± 6	381 ± 7	272 ± 7
HELMS2 [‡]	23 ^h 32 ^m 55 ^s .4	−03°11′34″	271 ± 6	336 ± 6	263 ± 8
HELMS3	00 ^h 02 ^m 15 ^s .9	−01°28′29″	643 ± 7	510 ± 6	258 ± 7
HELMS4 ^{*,†}	00 ^h 44 ^m 10 ^s .2	+01°18′21″	113 ± 7	177 ± 6	209 ± 8
HELMS5 [‡]	23 ^h 40 ^m 51 ^s .5	−04°19′38″	151 ± 6	209 ± 6	205 ± 8
HELMS6	23 ^h 36 ^m 20 ^s .8	−06°08′28″	193 ± 7	252 ± 6	202 ± 8
HELMS7 [‡]	23 ^h 24 ^m 39 ^s .5	−04°39′36″	214 ± 7	218 ± 7	172 ± 9
HELMS8 [‡]	00 ^h 47 ^m 14 ^s .2	+03°24′54″	312 ± 6	244 ± 7	168 ± 8
HELMS9 [‡]	00 ^h 47 ^m 23 ^s .6	+01°57′51″	398 ± 6	320 ± 6	164 ± 8
HELMS10 [*]	00 ^h 52 ^m 58 ^s .6	+06°13′19″	88 ± 6	129 ± 6	155 ± 7
HELMS11 ^{*,†}	00 ^h 39 ^m 29 ^s .6	+00°24′26″	140 ± 7	157 ± 7	154 ± 8
HELMS12	23 ^h 56 ^m 01 ^s .5	−07°11′42″	178 ± 7	184 ± 6	154 ± 7
HELMS13 [‡]	00 ^h 16 ^m 15 ^s .7	+03°24′35″	195 ± 6	221 ± 6	149 ± 7
HELMS14	00 ^h 36 ^m 19 ^s .8	+00°24′20″	251 ± 6	247 ± 6	148 ± 7
HELMS15 [‡]	23 ^h 32 ^m 55 ^s .7	−05°34′26″	148 ± 6	187 ± 6	147 ± 9
HELMS16	23 ^h 18 ^m 57 ^s .2	−05°30′35″	143 ± 7	183 ± 7	146 ± 8
HELMS17	23 ^h 25 ^m 58 ^s .3	−04°45′25″	190 ± 6	189 ± 6	142 ± 8
HELMS18 [‡]	00 ^h 51 ^m 59 ^s .5	+06°22′41″	166 ± 6	195 ± 6	135 ± 7
HELMS19	23 ^h 22 ^m 10 ^s .3	−03°35′59″	114 ± 6	160 ± 7	134 ± 8
HELMS20	23 ^h 37 ^m 28 ^s .8	−04°51′06″	162 ± 6	178 ± 7	132 ± 8
HELMS21	00 ^h 18 ^m 00 ^s .1	−06°02′35″	206 ± 6	186 ± 7	130 ± 7
HELMS22 [‡]	00 ^h 16 ^m 26 ^s .0	+04°26′13″	117 ± 7	151 ± 6	127 ± 7
HELMS23	00 ^h 58 ^m 41 ^s .2	−01°11′49″	391 ± 7	273 ± 6	126 ± 8
HELMS24 ^{*,†}	00 ^h 38 ^m 14 ^s .1	−00°22′52″	82 ± 6	120 ± 6	126 ± 7
HELMS25	00 ^h 41 ^m 24 ^s .0	−01°03′07″	178 ± 6	186 ± 7	125 ± 8
HELMS26 [*]	00 ^h 47 ^m 47 ^s .1	+06°14′44″	85 ± 7	119 ± 6	125 ± 8
HELMS27	00 ^h 37 ^m 58 ^s .0	−01°06′22″	125 ± 7	144 ± 6	124 ± 8
HELMS28	00 ^h 30 ^m 09 ^s .2	−02°06′25″	114 ± 6	135 ± 6	122 ± 7
HELMS29 ^{*,†}	00 ^h 22 ^m 20 ^s .9	−01°55′24″	66 ± 6	102 ± 6	121 ± 7
HELMS30	00 ^h 10 ^m 27 ^s .1	−02°46′24″	185 ± 6	170 ± 6	121 ± 7
HELMS31	00 ^h 13 ^m 53 ^s .5	−06°02′00″	178 ± 7	176 ± 6	120 ± 7
HELMS32	00 ^h 03 ^m 36 ^s .9	+01°40′13″	103 ± 6	112 ± 6	119 ± 7
HELMS33	00 ^h 30 ^m 32 ^s .1	−02°11′53″	81 ± 7	98 ± 6	118 ± 8
HELMS34	00 ^h 27 ^m 19 ^s .5	+00°12′04″	248 ± 6	206 ± 7	116 ± 8
HELMS35	23 ^h 25 ^m 00 ^s .1	−00°56′43″	122 ± 6	132 ± 7	114 ± 8
HELMS36	23 ^h 43 ^m 14 ^s .0	+01°21′52″	115 ± 6	115 ± 6	113 ± 8
HELMS37	01 ^h 08 ^m 01 ^s .8	+05°32′01″	122 ± 6	120 ± 6	113 ± 7
HELMS38	00 ^h 22 ^m 08 ^s .1	+03°40′44″	190 ± 6	157 ± 6	113 ± 7
HELMS39	00 ^h 29 ^m 36 ^s .3	+02°07′10″	81 ± 6	107 ± 6	112 ± 7
HELMS40 [‡]	23 ^h 53 ^m 32 ^s .0	+03°17′18″	102 ± 6	123 ± 7	111 ± 7
HELMS41	23 ^h 36 ^m 33 ^s .5	−03°21′19″	130 ± 6	131 ± 6	110 ± 7
HELMS42	23 ^h 40 ^m 14 ^s .6	−07°07′38″	158 ± 6	154 ± 6	110 ± 8
HELMS43	23 ^h 34 ^m 20 ^s .4	−00°34′58″	156 ± 7	141 ± 5	109 ± 8
HELMS44	23 ^h 14 ^m 47 ^s .5	−04°56′58″	220 ± 8	141 ± 7	106 ± 8
HELMS45	00 ^h 12 ^m 26 ^s .9	+02°08′10″	107 ± 6	142 ± 6	106 ± 7
HELMS46	00 ^h 46 ^m 22 ^s .3	+07°35′09″	82 ± 9	113 ± 9	105 ± 10
HELMS47	23 ^h 49 ^m 51 ^s .6	−03°00′19″	186 ± 7	167 ± 6	105 ± 8
HELMS48	23 ^h 28 ^m 33 ^s .6	−03°14′16″	49 ± 6	104 ± 6	105 ± 8
HELMS49	23 ^h 37 ^m 21 ^s .9	−06°47′40″	173 ± 6	161 ± 7	105 ± 8
HELMS50	23 ^h 51 ^m 01 ^s .7	−02°44′26″	112 ± 6	124 ± 6	105 ± 7
HELMS51	23 ^h 26 ^m 17 ^s .5	−02°53′19″	86 ± 6	109 ± 6	104 ± 7
HELMS52	23 ^h 37 ^m 27 ^s .1	−00°23′43″	182 ± 6	157 ± 6	104 ± 8
HELMS53 [‡]	00 ^h 45 ^m 32 ^s .6	−00°01′23″	48 ± 7	85 ± 6	103 ± 8
HELMS54	00 ^h 27 ^m 18 ^s .1	+02°39′43″	69 ± 6	87 ± 6	103 ± 7
HELMS55	23 ^h 28 ^m 31 ^s .8	−00°40′35″	95 ± 7	120 ± 6	102 ± 7
HELMS56	00 ^h 13 ^m 25 ^s .7	+04°25′09″	89 ± 6	98 ± 6	102 ± 7
HELMS57	00 ^h 35 ^m 19 ^s .7	+07°28′06″	134 ± 6	135 ± 7	101 ± 8

*: Red source in Asboth et al. (2016)

†: ACT identified lensed DSFG (Su et al. 2015)

‡: ALMA Cycle 1 targets (PI: Eales)

Table 3 HerS lens candidates ($S_{500} > 100$ mJy)

Object ID	RA	Dec	S_{250} (mJy)	S_{350} (mJy)	S_{500} (mJy)
HERS1 ^{*,†}	02 ^h 09 ^m 41 ^s .2	+00°15′58″	826 ± 7	912 ± 7	718 ± 8
HERS2	01 ^h 20 ^m 41 ^s .6	−00°27′05″	240 ± 6	260 ± 6	198 ± 7
HERS3	01 ^h 27 ^m 54 ^s .1	+00°49′40″	253 ± 6	250 ± 6	191 ± 7
HERS4 [†]	01 ^h 16 ^m 40 ^s .1	−00°04′54″	137 ± 7	196 ± 7	190 ± 8
HERS5	01 ^h 26 ^m 20 ^s .5	+01°29′50″	268 ± 8	228 ± 7	133 ± 9
HERS6	01 ^h 03 ^m 01 ^s .2	−00°33′01″	121 ± 7	147 ± 6	130 ± 8
HERS7	01 ^h 01 ^m 33 ^s .8	+00°31′57″	165 ± 7	154 ± 6	122 ± 7
HERS8	01 ^h 09 ^m 38 ^s .9	−01°48′30″	146 ± 8	152 ± 7	118 ± 10
HERS9	01 ^h 09 ^m 11 ^s .7	−01°17′33″	393 ± 8	220 ± 8	118 ± 9
HERS10	01 ^h 17 ^m 22 ^s .3	+00°56′24″	105 ± 6	125 ± 6	117 ± 7
HERS11	00 ^h 58 ^m 47 ^s .3	−01°00′17″	63 ± 8	116 ± 7	115 ± 9
HERS12	01 ^h 25 ^m 46 ^s .3	−00°11′43″	152 ± 8	135 ± 7	114 ± 9
HERS13	01 ^h 25 ^m 21 ^s .0	+01°17′24″	165 ± 8	153 ± 7	114 ± 10
HERS14	01 ^h 40 ^m 57 ^s .3	−01°05′47″	136 ± 8	143 ± 8	112 ± 9
HERS15	01 ^h 21 ^m 06 ^s .9	+00°34′57″	94 ± 6	130 ± 7	110 ± 7
HERS16	02 ^h 14 ^m 34 ^s .4	+00°59′26″	110 ± 9	134 ± 8	109 ± 10
HERS17	02 ^h 14 ^m 02 ^s .6	−00°46′12″	110 ± 8	130 ± 8	105 ± 9
HERS18	01 ^h 32 ^m 12 ^s .2	+00°17′54″	176 ± 7	175 ± 6	104 ± 8
HERS19	02 ^h 05 ^m 29 ^s .1	+00°05′01″	89 ± 6	112 ± 6	102 ± 8
HERS20	01 ^h 02 ^m 46 ^s .1	+01°05′43″	107 ± 8	133 ± 8	102 ± 11

*: Lensed sources identified in Geach et al. (2015)

†: ACT identified lensed DSFG (Su et al. 2015)

Table 4 Properties of the foreground lensing galaxy and background lensed submillimeter galaxy.

ID	Name	z (foreground) ¹	z (SMG)
HERS1	HERS J020941.1+001557	0.202 ² ± 0.00006	2.553 ³
HELMS2	HERMES J233255.5-031134	0.426 ± 0.1483	2.6899 ⁴
HELMS5	HERMES J234051.3-041937	—	3.50 ⁵
HELMS6	HERMES J233620.7-060826	0.3958 ⁶ ± 0.0007	3.434 ⁵
HERS2	HERS J012041.5-002705	0.732 ± 0.0406	—
HERS4	HERS J011640.0-000453	0.445 ± 0.0612	—
HELMS7	HERMES J232439.4-043934	—	2.473 ⁴
HELMS8	HERMES J004714.1+032453	0.478 ± 0.0847	1.19 ⁵
HELMS9	HERMES J004723.3+015749	0.299 ± 0.0542	1.441 ⁵
HELMS10	HERMES J005258.6+061317	0.241 ± 0.1176	—
HELMS12	HERMES J235601.5-071144	0.775 ± 0.0800	—
HELMS13	HERMES J001615.8+032433	0.663 ² ± 0.00025	2.765 ⁴
HELMS14	HERMES J003619.7+002420	0.258 ² ± 0.00005	—
HELMS15	HERMES J233255.7-053424	0.976 ± 0.0565	2.4024 ⁴
HELMS18	HERMES J005159.4+062240	—	2.392 ⁴
HELMS19	HERMES J232210.3-033600	0.143 ± 0.0869	—
HERS5	HERS J012620.5+012949	0.431 ± 0.0495	—
HELMS21	HERMES J001800.1-060234	0.574 ± 0.1237	—
HERS6	HERS J010301.2-003300	0.429 ² ± 0.00010	2.2153 ⁴
HELMS22	HERMES J001626.0+042613	0.218 ± 0.0175	2.5093 ⁴
HELMS23	HERMES J005841.0-011148	0.375 ± 0.0777	—
HELMS24	HERMES J003813.9-002253	0.169 ± 0.0846	—
HELMS25	HERMES J004123.8-010311	0.271 ± 0.0716	—
HELMS28	HERMES J003009.2-020623	0.415 ± 0.1188	—
HERS7	HERS J010133.7+003157	0.334 ± 0.1205	—
HELMS29	HERMES J002220.9-015520	—	5.162 ⁷
HELMS30	HERMES J001027.1-024625	0.851 ± 0.1137	—
HELMS31	HERMES J001353.6-060200	0.604 ± 0.1777	—
HERS8	HERS J010938.8-014829	0.378 ± 0.0821	—
HERS9	HERS J010911.7-011732	0.853 ² ± 0.00008	—
HERS10	HERS J011722.2+005624	0.873 ± 0.0531	—
HELMS34	HERMES J002719.6+001203	0.512 ± 0.1403	—
HERS11	HERS J005847.2-010016	0.717 ± 0.1537	—
HELMS35	HERMES J232500.1-005644	0.299 ± 0.1217	—
HERS12	HERS J012546.3-001143	0.893 ² ± 0.00039	—
HELMS36	HERMES J234314.0+012152	0.489 ± 0.0286	—
HELMS38	HERMES J002207.9+034044	0.217 ² ± 0.00004	—
HERS14	HERS J014057.3-010547	0.370 ± 0.0724	—
HELMS39	HERMES J002936.3+020706	0.770 ± 0.1217	—

Table 4 Properties of the foreground lensing galaxy and background lensed submillimeter galaxy.

ID	Name	z (foreground) ¹	z (SMG)
HELMS40	HERMES J235331.7+031717	0.821 ± 0.0940	–
HERS15	HERS J012106.8+003456	0.698 ± 0.0721	–
HELMS42	HERMES J234014.4-070737	0.460 ± 0.0487	–
HELMS43	HERMES J233420.2-003455	0.139 ± 0.0591	–
HERS16	HERS J021434.4+005925	0.492 ± 0.1321	–
HELMS44	HERMES J231447.6-045657	0.451 ± 0.0816	–
HELMS46	HERMES J004622.2+073514	0.442 ± 0.1621	–
HERS17	HERS J021402.5-004612	$0.369^2 \pm 0.00012$	–
HELMS50	HERMES J235101.7-024425	$0.134^2 \pm 0.00002$	–
HERS18	HERS J013212.2+001754	0.495 ± 0.0755	–
HERS19	HERS J020529.0+000500	0.455 ± 0.0764	–
HELMS56	HERMES J001325.8+042506	0.485 ± 0.1861	–
HELMS57	HERMES J003519.7+072808	0.094 ± 0.1104	–

¹: SDSS DR12 PhotoZ KD tree method, unless otherwise noted

²: SDSS DR12 Spectroscopic Redshift

³: Geach et al. 2015

⁴: GBT/Zspectrometer (Harris et al., in prep), CARMA and PdBI (Riechers et al., in prep)

⁵: CARMA and PdBI (Riechers et al., in prep)

⁶: GTC/OSIRIS spectroscopic redshift, Marques-Chaves et al., in prep

⁷: Asboth et al. (2016)

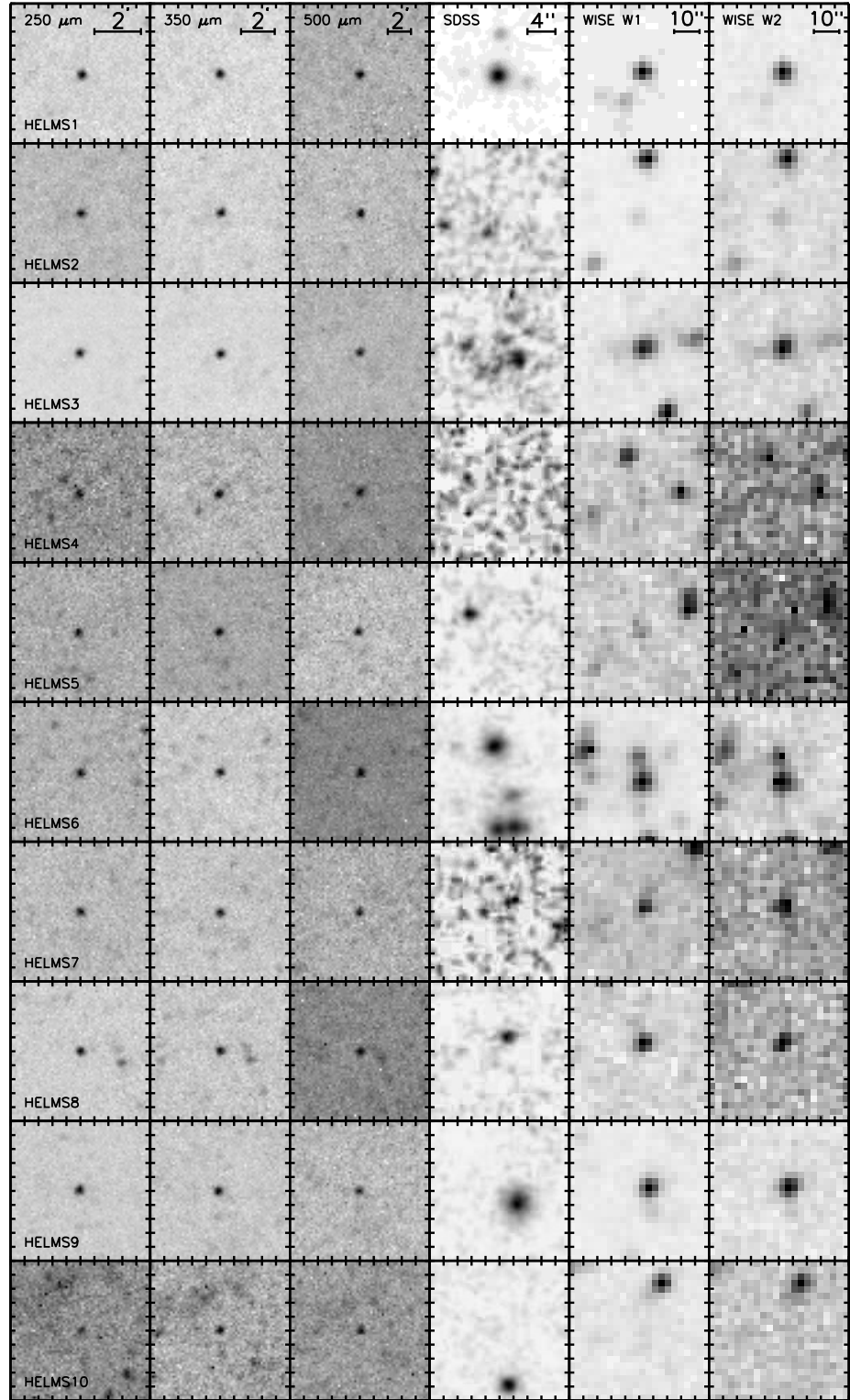


Figure 9. The postage stamp images of the candidate gravitationally lensed DSFGs in the HeLMS field in the *Herschel* far-infrared, SDSS optical and Wide-field Infrared Survey Explorer (WISE; Wright et al. 2010) infrared bands. The *Herschel* cutouts are from our SANEPIC maps (see Asboth et al. 2016) with the coordinates derived from the higher resolution $250\,\mu\text{m}$ observations. The SDSS data are from deep co-adds by Jiang et al. (2014) when available and single epoch observations from SDSS DR12, when deeper data is not available. The infrared data are in WISE W1 (at $3.4\,\mu\text{m}$) and W2 (at $4.6\,\mu\text{m}$) bands using unWISE images (Lang 2014). The image scales are shown for the first row. The lensed candidates are point-like bright targets in the *Herschel* SPIRE cutouts. The SDSS and WISE cutouts show the lensing foreground galaxies.

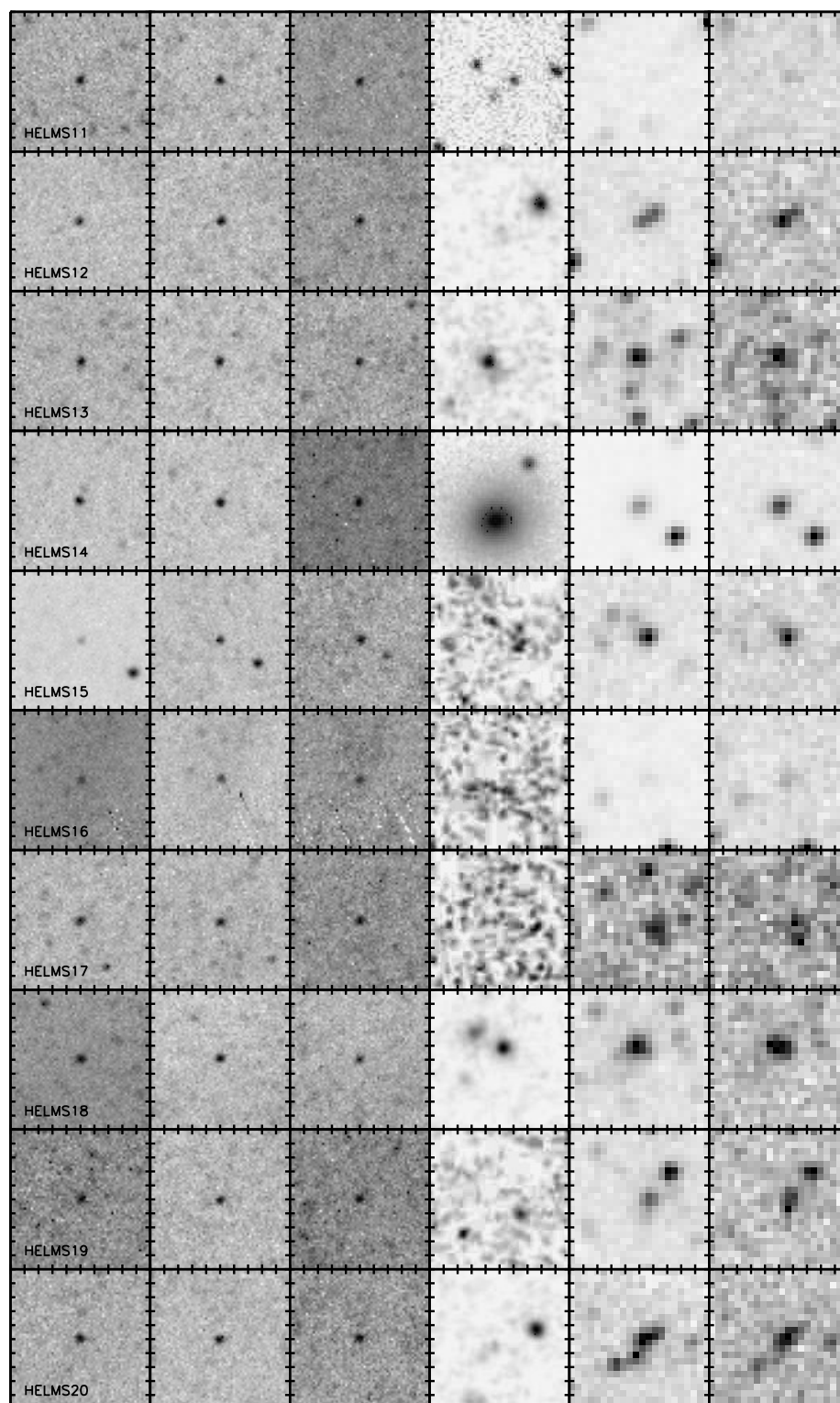


Figure 9. Continued.

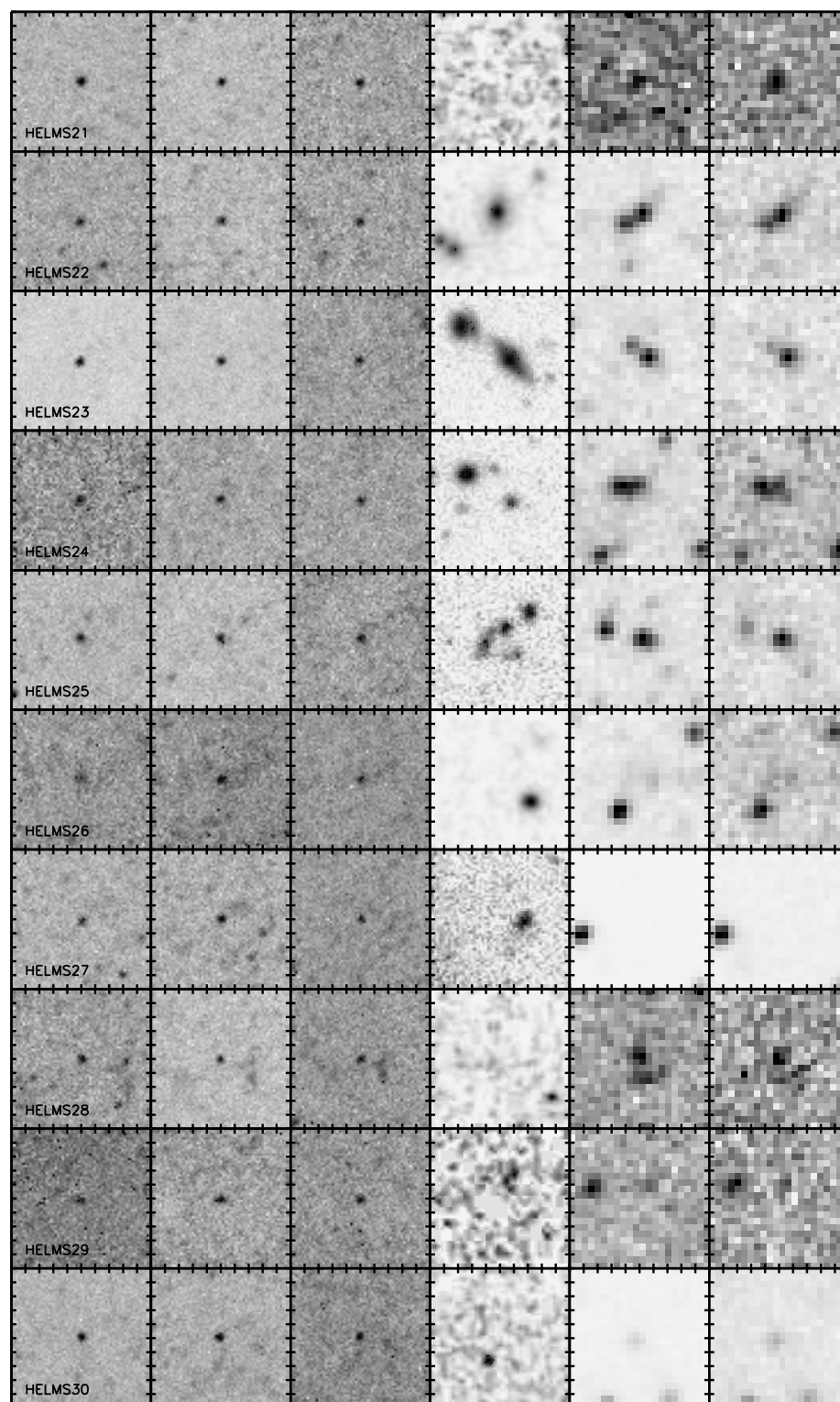


Figure 9. Continued.

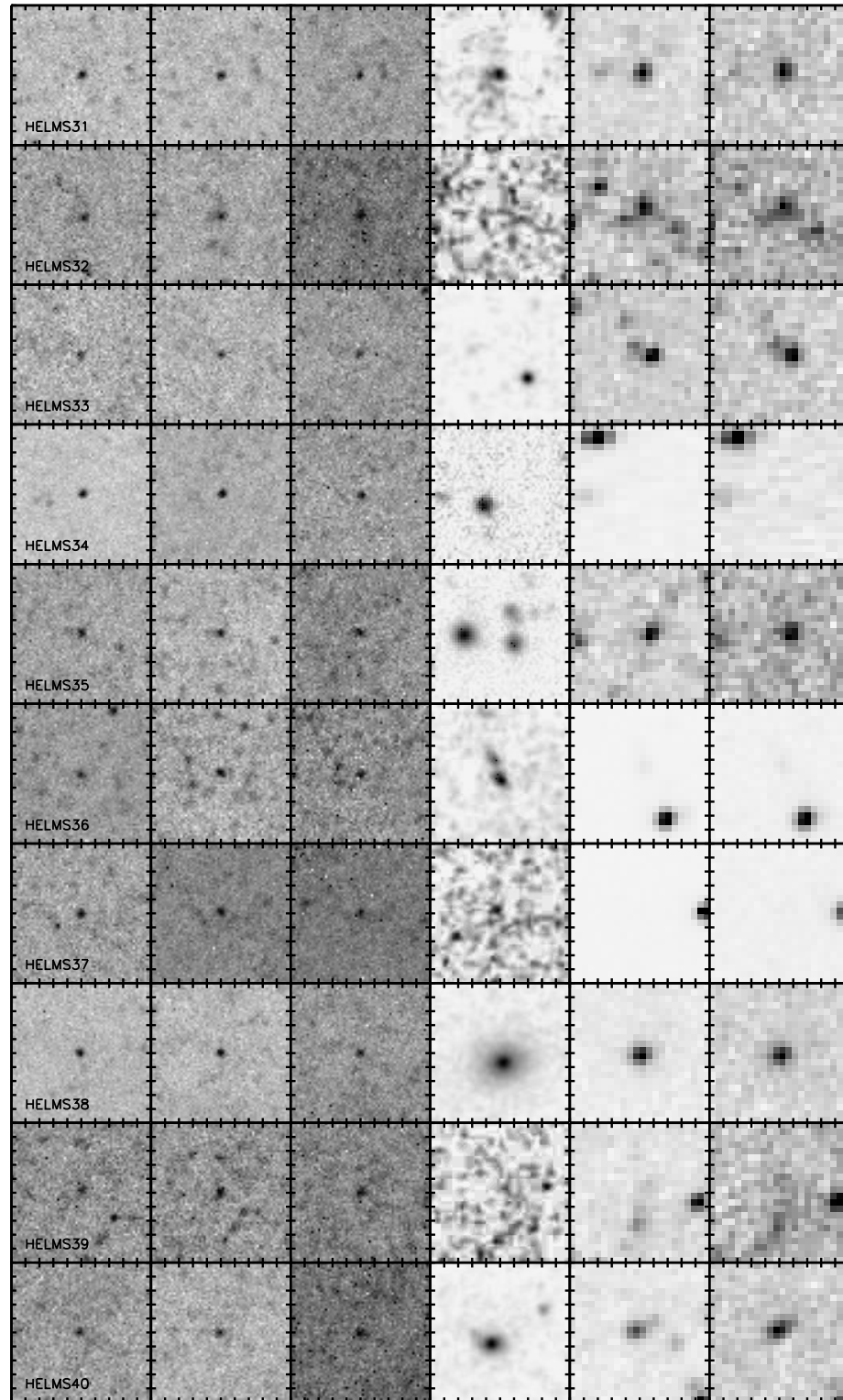


Figure 9. Continued.

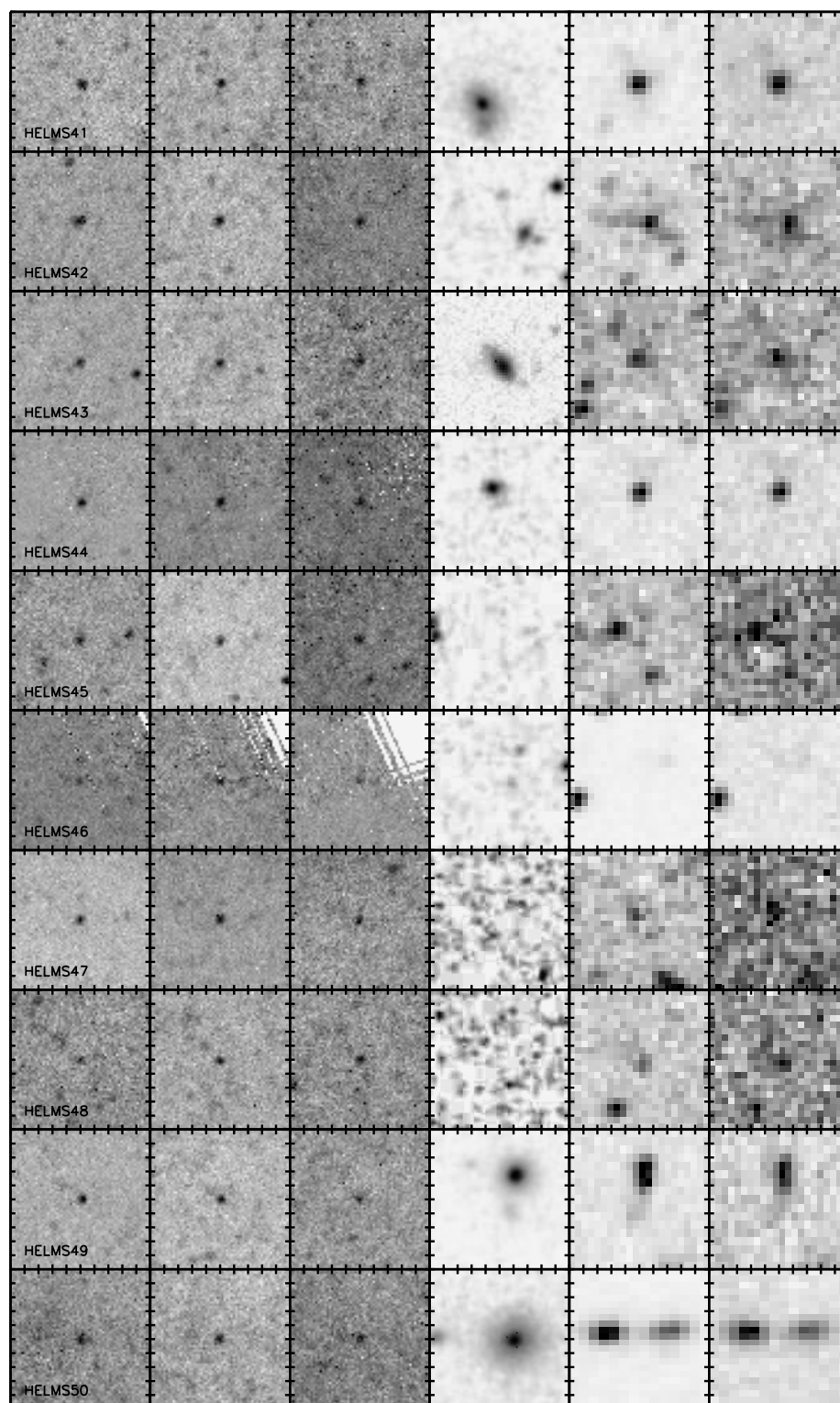


Figure 9. Continued.

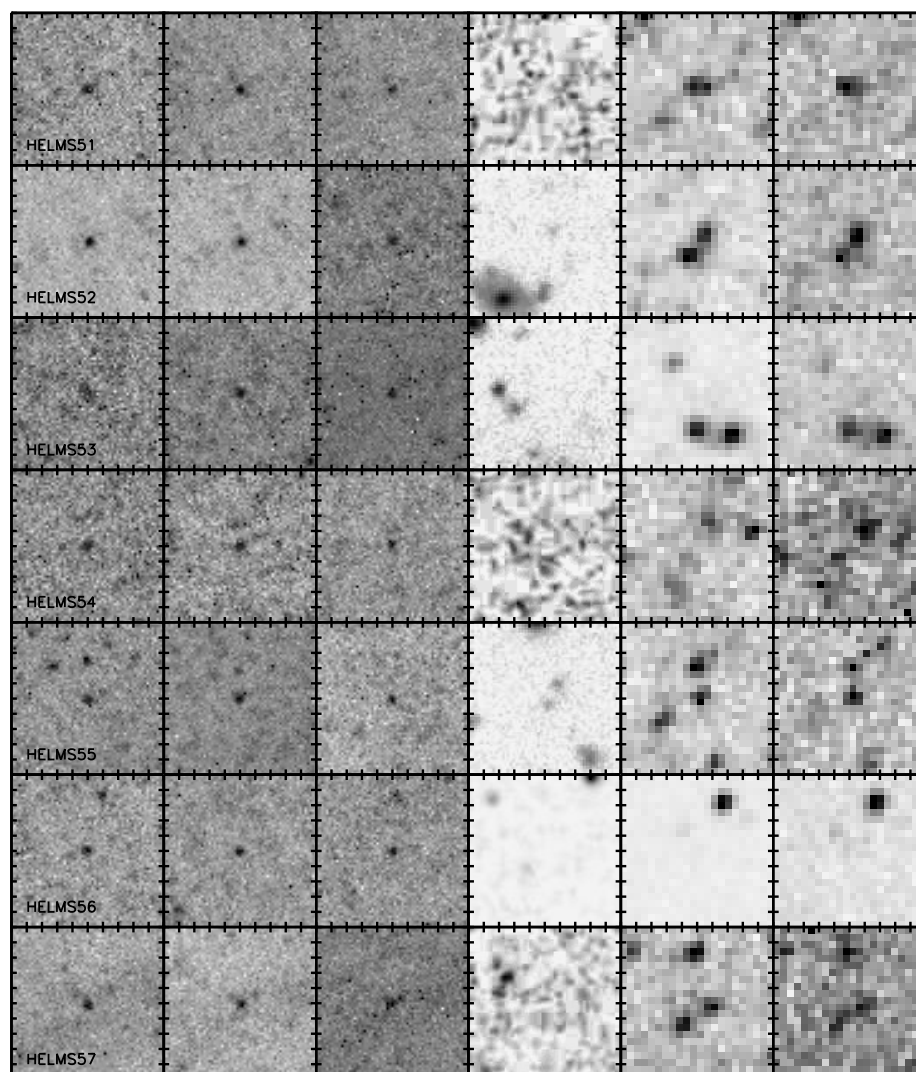


Figure 9. Continued.

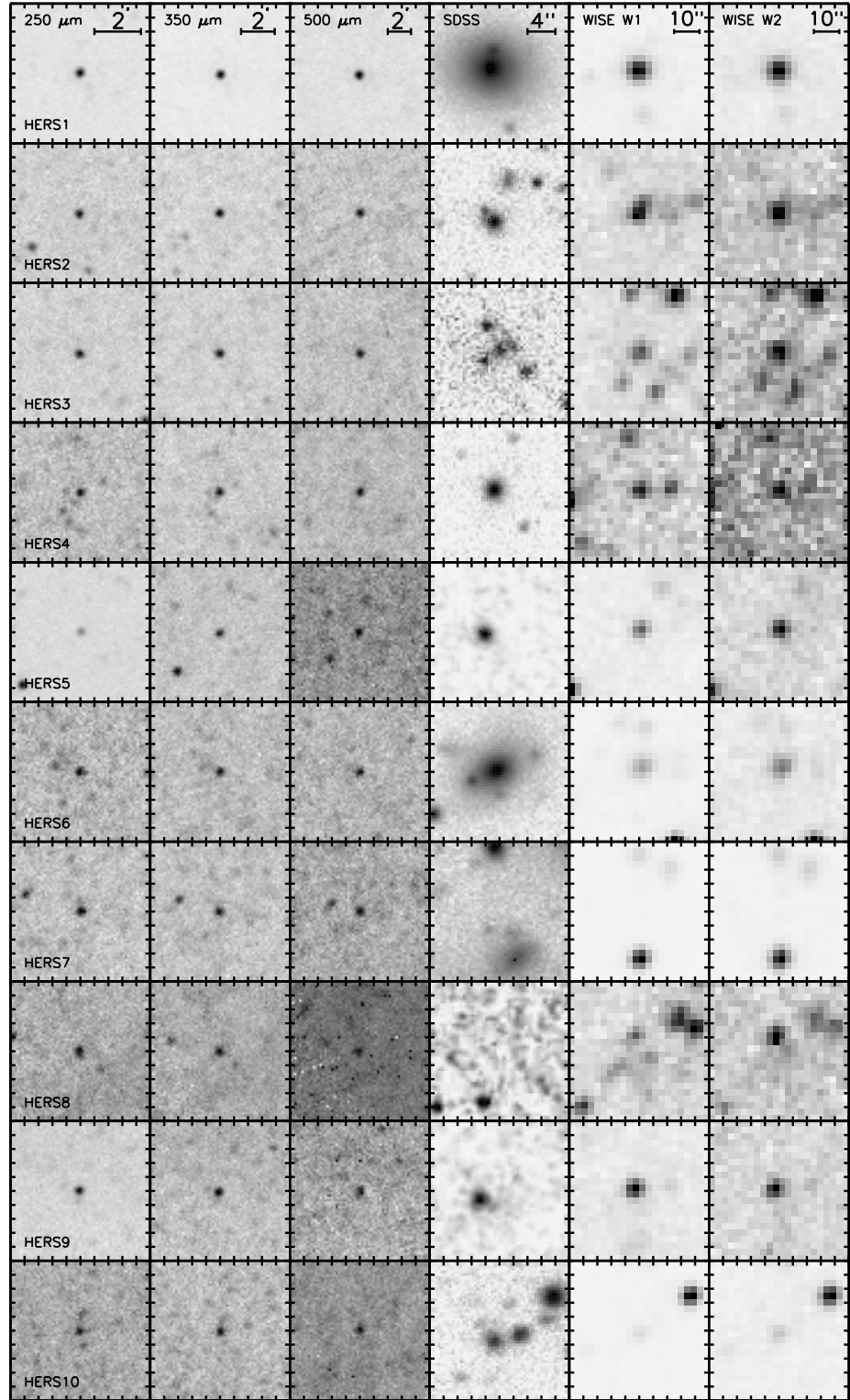


Figure 10. Same as Figure 9 but for the HerS sample of gravitationally lensed DSFG candidates.

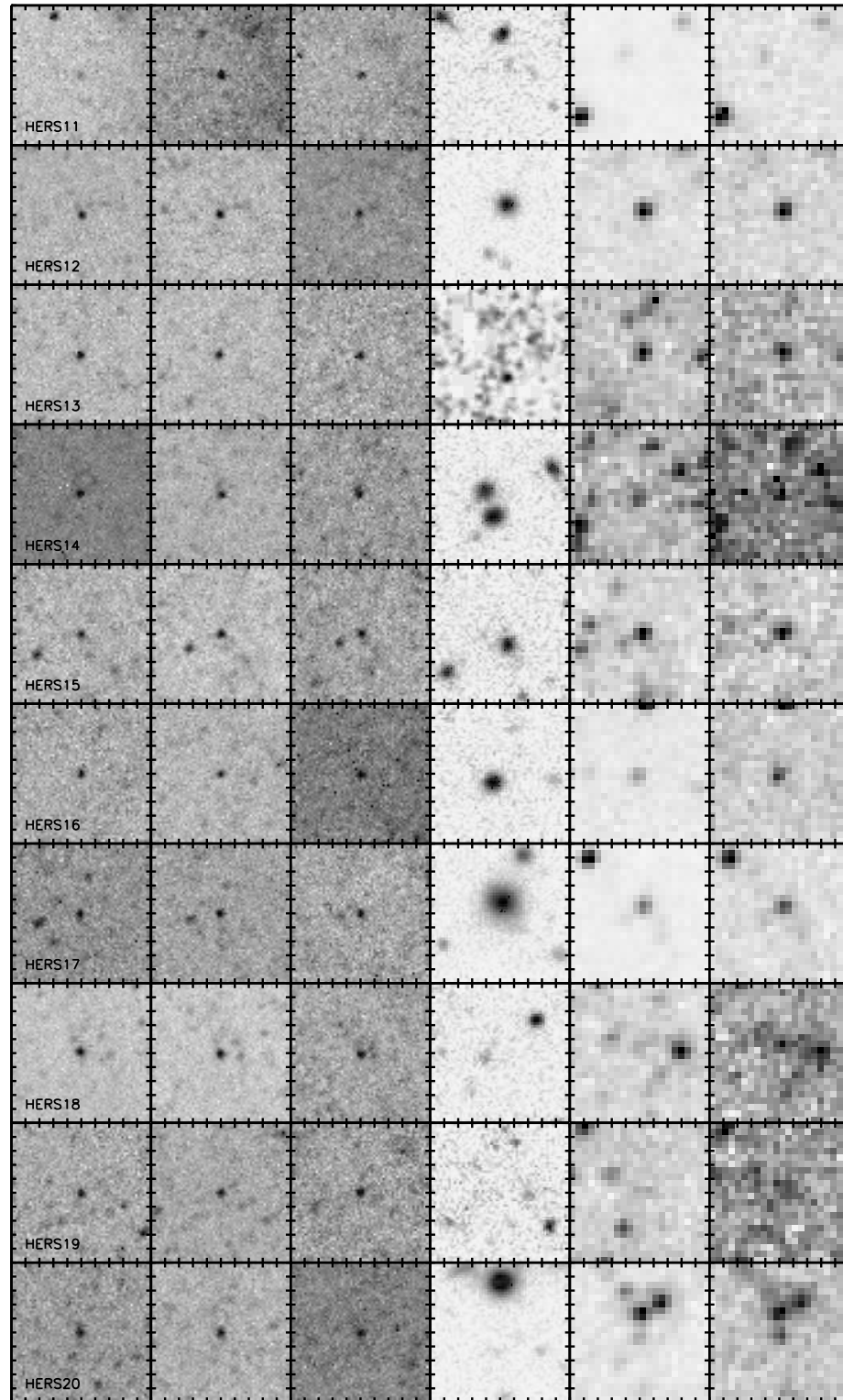


Figure 10. Continued.